A Diverted Submarine Channel of Early Cretaceous Age Revealed by High-Resolution Seismic Data, SW Barents Sea

[UNCORRECTED PROOF VERSION]
September 2018, Marine and Petroleum Geology 98
DOI: 10.1016/j.marpetgeo.2018.08.037

Romain Corseri[1,*], Thea Sveva Faleide[1,2], Jan Inge Faleide[2,3], Ivar Midtkandal[2], Christopher Sæbø Serck[2] , Mikal Trulsvik[1,4], Sverre Planke[1,3]

[1]Volcanic Basin Petroleum Research AS, Oslo Science Park, Gaustadalléen 21, N-0349 Oslo, Norway

[2]University of Oslo, Department of Geosciences, University of Oslo, Box 1047 Blindern, 0316 Oslo, Norway

[3]Center for Earth Evolution and Dynamics, University of Oslo, Box 1028 Blindern, 0315 Oslo, Norway

[4]TGS, Lensmannslia 4, 1386 Asker, Norway

[*]Corresponding author: romain.corseri@gmail.com / romain@vbpr.no - Mob: +47 97487906

Abstract

Mud-rich prograding sediment lobes make for most of the Barremian – Albian stratigraphic record in the SW Barents Sea. Submarine canyons and channels potentially represent key components of sediment transport from shelf to basin floor but geological evidences are lacking. We present high-resolution seismic data and scrutinize an elongated, ~150-km long bright seismic amplitude and resistive anomaly located alongslope of a NW-sourced Barremian delta in the SW Barents Sea. Seismic interpretation is performed on a comprehensive database comprising 3D/2D high-resolution P-Cable and conventional seismic data, tied to three exploration wells to provide age-control on key horizons. Our results highlight that the elongated geophysical anomaly originates from a soft layer deposited over a harder, erosional surface. The erosive morphology displays three narrow, V-shaped incisions to the NE of the Hoop area which develop into a single, ~6 km-wide U-shape channel towards the transition to the Fingerdjupet Subbasin. The geological feature is named Ceres and interpreted as a submarine channel carved in Aptian, a period of marked sea level rise and sediment starvation in the Hoop area. An evolutionary model of a diverted submarine channel is proposed where a flooded delta lobe acted as a topographic barrier, funneling bottom currents and thereby carving an alongslope, possibly contouritic channel. This is the first documented case of a submarine channel pathway – delta lobe interaction on the Norwegian continental shelf. To account for the geophysical expression of Ceres, two competing explanations are discussed: (1) hydrocarbon-bearing sands, and (2) organic-rich source rock. Both scenarios have important implications for petroleum prospectivity: a faulted stratigraphic trap holding large volumes of hydrocarbons or alternatively the channel-controlled distribution of mature Aptian source rock in the SW Barents Sea.

Keywords

Early Cretaceous; SW Barents Sea; High-resolution seismic data; Submarine channel; Contouritic currents; Hydrocarbon; Source rock; Resistivity

1. Introduction

The understanding of sediment transport mechanism from shelf to basin floor is key to predict facies associations in the Lower Cretaceous strata of the Barents Sea. Fine-grained, marine mudstones make for most of the Lower Cretaceous stratigraphic record of the SW Barents Sea (Smelror et al., 2009) and the presence of reservoir rocks is an important factor affecting the potential of the Lower Cretaceous play. The depositional dynamics of the Early Cretaceous epicontinental sea is consequently under scrutiny (Harishiyadat et al., 2018; Marín et al., 2018; Grundvåg et al., 2017; Marín et al., 2017; Midtkandal et al., 2014). Submarine canyons and channels are key elements in the discharge of sand from shelf to basin floor but evidences are lacking (Marin et al., 2017) in the SW Barent Sea. The high-resolution P-Cable seismic data presented here could potentially resolve subtle incisions and help tracking sand-prone sediment conduits.

As the petroleum industry investigates Lower Cretaceous targets, recent hydrocarbon discoveries have confirmed the potential of the Cretaceous play in the SW Barents Sea. Indeed, The Kayak well (73219/9-2) proved oil in a Lower Cretaceous clastic wedge and potential tie-in of the discovery to Johan Castberg field development is being assessed (NPD, 2017). Located ~170 km northwest of Johan Castberg's discoveries, the Hoop area (Fig. 1) is mature area for exploration as sizeable hydrocarbon discoveries were made in the Jurassic-Late Triassic Realgrunnen Subgroup: Wisting (7324/8-1), Hanssen (7324/7-2), Gemini North (7324/9-1) and Mercury (7325/4-1). In this area, integrated interpretation of seismic and Controlled-Source Electromagnetic (CSEM) data have proven to be an efficient de-risking tool (Alvarez et al., 2018; Granli et al., 2017; Fanavoll et al., 2014) because of the extremely high resistivity in the oil- and gas-saturated reservoir sands (Senger et al., 2017). Indeed, all the aforementioned discoveries were associated with coincident Direct Hydrocarbon Indicators (DHI), a high amplitude event in seismic data and a resistive anomaly from 3D inversion of CSEM data. This

work scrutinizes Ceres, a elongated high acoustic amplitude event associated with a prominent resistive anomaly (Fig. 2a) originating from the Lower Cretaceous interval (Fig. 2b). The specificity of Ceres lies also in its close stratigraphic relationship with a pre-existing delta lobe front, potentially acting as a bathymetric obstacle for bottom currents in the Early Cretaceous epicontinental sea.

This study has four aims: (1) to map, describe and interpret a prominent elongated anomaly in Lower Cretaceous strata based in 3D/2D high-resolution P-Cable and conventional seismic data, (2) to understand the stratigraphic relationship between this enigmatic elongated feature and the underlying or overlying Lower Cretaceous prograding units, (3) to develop the first geological interpretation of an ancient submarine channel in the Hoop area, constraining its morphology, timing and internal fill, and (4) to propose an Early Cretaceous paleo-geographic reconstruction of the study area and discuss implications for petroleum prospectivity.

This contribution will be articulated in four parts. First, we review the recent updates in Lower Cretaceous stratigraphic framework and basin development of the NW Bjarmeland Platform and Fingerdjupet Subbasin. Secondly, we introduce the seismic database and elaborate on the seismic interpretation methodology, starting from regional seismic interpretation and gradually zooming-in using a combination of 2D and 3D high-resolution data tied to key exploration wells. Based on these observations, we develop an evolutionary model constraining the timing, infill and diverted course of a submarine channel contouring a flooded Barremian delta lobe front. Eventually, this work envisions the presence of a sediment fairway in the SW Barents Sea, conveying bypassed products from NE to SW through a submarine channel in Aptian.

2. Geological framework

2.1 Early Cretaceous structural setting and basin architecture

Prior to the opening of the NE Atlantic in Early Cenozoic time, the Barents epicontinental shelf was surrounded by continental land masses of Fennoscandia, Greenland, Svalbard and Novaya Zemlya (Grundvåg et al., 2017). Throughout Late Paleozoic and Mesozoic times, the Barents Sea was under extension, characterized by several N-S to NE-SW trending rift basins and structural highs (Faleide et al., 1993; Gudlaugsson et al., 1998; Indrevær et al., 2017; Serck et al., 2017). The area of interest is the Hoop area, located in the SW Barents Sea and adjacent to the Fingerdjupet Subbasin (Fig. 1). The latter forms the northeastern transition to the deep Bjørnøya Basin. In Early Cretaceous, the Fingerdjupet Subbasin experienced significant subsidence resulting in thicker successions of Lower Cretaceous strata compared to adjacent structural highs (Serck et al., 2017). In this period, the highs and platforms, such as the Hoop area, were sediment-starved and locally developed carbonate successions, the Klippfisk Formation (Smelror et al., 1998). The post-Early Cretaceous uplift episodes (Baig et al., 2016; Dimakis et al., 1998; Green et al., 2010; Henriksen et al., 2011b), intensified by Pleistocene glacio-erosive processes (Sættem et al., 1992; Laberg et al., 2012; Bellwald et al., 2018), have removed much of the Lower Cretaceous deposits on the structural highs. Beside, a part of the depocenter was uplifted in Early Barremian to form a subaerially-exposed platform corresponding to the present day Loppa High (Fig. 1; Indrevær et al., 2016; Indrevær et al., 2017).

2.2 Lower Cretaceous stratigraphy

A lithostratigraphic and seismic stratigraphic framework of the Upper Jurassic to Lower Cretaceous in the Bjarmeland Platform is shown in Fig. 3, based on Midtkandal et al. (2016). The Cretaceous succession (Fig. 3) is subdivided into the mudstone-dominated Knurr, Kolje and Kolmule formations. The potential for reservoir quality sandstones is believed to be mostly

limited to thin sandstone sheets (Grundvåg et al., 2017). A description of each sequence based on public data (NPD, 2017) is summarized below.

Knurr Formation (Berriasian-Early Barremian): The Knurr Formation consists of claystone, thin interbeds of limestone/dolomite and thin sandstones in its lower part distributed on the Bjarmeland Platform. The Knurr Formation is time-equivalent to the carbonate dominated Klippfisk Formation. The latter was deposited in shallow marine platform areas and local structural highs (Smelror et al., 1998).

Kolje Formation (Barremian-Early Aptian): The Kolje Formation overlies the Knurr Formation with a sharp and in places erosive boundary. The Kolje Formation is dominated by mudstone with thin interbeds of silt- and sandstone and lateral equivalent to the sandstone-dominated Helvetiafjellet Formation on Spitsbergen (NPD, 2017).

Kolmule Formation (Aptian-Mid Cenomanian): Details on the Kolmule Formation from the Bjarmeland Platform are scarce, but the formation is considered to be dominated by mudstone with thin siltstone, limestone interbeds and dolomite stringers, indicating an open-marine deposition (NPD, 2017).

2.3 Early Cretaceous basin infill history

In Early Cretaceous, the Barents Sea was an epicontinental sea under shelfal conditions. In such environment, the sediment transport and routing is influenced by subtle sea level changes and intrabasinal tectonics. In fact, the injection of magma in the lithosphere, at the onset of the High Arctic Large Igneous Province (HALIP), caused the northern portion of the Barents Sea shelf to be uplifted in Barremian to Early Aptian, resulting in the widespread progradation of sedimentary units to offshore areas (Polteau et al., 2016).

The distribution, geometry and age of Cretaceous prograding sequences in the western Barents Sea have been scrutinized by Dimitriou (2014), Midtkandal et al. (2014), Hinna (2016), Marín et al. (2017), and Grundvåg et al. (2017) using seismic and well data. Although the interpretation of lobes may vary in terms of lateral extent and age estimate amongst the latter studies, there is a wide consensus that Hauterivian-Barremian lobes filling the epicontinental basin are predominantly mud-rich, accomodating long-distance sediment transport from a major source area NW of Svalbard. In addition, lobes with a high-relief, oblique geometry and sourced from the Russian Barents Sea, are generally interpreted as mud-rich, intra-shelf prism prograding units (Marín et al., 2017; Grundvåg et al., 2017). Palynological analysis of several exploration and shallow IKU (Institutt for kontinentalundersøkelse, now SINTEF) wells have shown that the lobes in the western Bjarmeland Platform are of Barremian to Cenomanian age (Århus, 1991; Midtkandal and Nystuen, 2009).

Recent studies based on a dense grid of regional 2D conventional seismic lines complemented by 3D conventional seismic and high-resolution seismic data have led to refinement in the description of prograding units infilling the Early Cretaceous Barents Sea (Hinna, 2016; Faleide, 2017). In Fig. 4, we reproduce the spatial distribution and introduce a new naming convention of the Cretaceous prograding units, reflecting the location of the sediment source relative to the study area. Four prograding units (NW2, NE1, NE2 and NE3)

in the western Bjarmeland Platform are relevant to this work and depicted in the study area (Fig. 4). In the Hoop area, the NW-SE prograding lobe (NW2) sourced from NW of present-day Svalbard is interpreted as a subaqueous delta with high-gradient sigmoidal clinoforms (Fig. 5; Faleide, 2017). It is denoted S1 and S2 in Marín et al. (2017) or named S1 and S3 in Grundvåg et al. (2017). The relief of NW2 is estimated to be 220-290 meters after decompaction in the Hoop area (Faleide, 2017; Fig. 5). NW2 is well-imaged in high-resolution seismic data and formed the Barremian prograding sequence in the Kolje Formation (Fig. 5). NE1, NE2 and NE3 are prograding sequences part of the Kolmule Formation and filled the study area from NE in Aptian to Albian (Dimitriou, 2014; Grundvåg et al., 2017; Marín et al., 2017).

2.4 Ceres: an elongated, high-amplitude and resistive anomaly in the Hoop area

The Lower Cretaceous interval in the study area shows prominent anomalies identified in two independent geophysical measurements: 3D Seismic and CSEM data (Fig. 2). The feature was ranked as a lead by Oil and Gas companies exploring the Hoop area. Following the nomenclature principles established in Gabrielsen et al. (1990), we have named the feature "Ceres" after the Norwegian polar research vessel "Ceres I" built in 1912. In the seismic data, a prominent elongated high-amplitude event, corresponding to negative impedance contrast (i.e. soft kick), is readily observable on a RMS attribute map for a 110 ms time-window defined above the BCU level (Fig. 2). This Cretaceous RMS amplitude anomaly stands out as a ~40 km long and 2-5 km wide feature, encompassing both stable platform and N-S graben structures (Fig. 2a). The high-amplitude, elongated seismic event seemingly extends farther west of the area displayed in Fig. 2. The contour of a highly resistive anomaly from Lower Cretaceous, extracted from Baltar and Barker (2017) and Carstens (2014), is overlain on the seismic anomaly in Fig. 2. The resistivity of the subsurface is retrieved from inversion of CSEM data, an exploration technique developed in the early 2000s (Constable and Weiss, 2006; Eidesmo et al., 2002) and intensively used for prospect de-risking in the Hoop area (Alvarez et al., 2018;

Granli et al., 2017; Fanavoll et al., 2014). Resistivity is an anisotropic property of the subsurface and is mainly controlled, in sedimentary basins, by (1) porosity (2) brine conductivity (inverse of resistivity) (3) pore space connectivity and, (4) brine saturation (Senger et al., 2017). Given the sensitivity of the CSEM method to Anomalous Transverse Resistance (ATR, i.e. the product of thickness and resistivity above a background level; Baltar and Roth, 2013), the information can be used to infer reservoir resistivity. When the reservoir thickness is known from seismic imaging, CSEM data can be used for pre-dill volumetric estimation (Baltar and Barker, 2015). In this contribution, the resistivity values of Ceres is not accessible and a more qualitative approach will be preferred for the CSEM-seismic data integration. In Fig. 2a, the seismic amplitude and highly resistive anomalies from CSEM data are roughly coincident with minor discrepancies in shape and lateral extent. Importantly, both anomalies embrace the contour of the delta lobe front NW2 in the study area (Fig. 4). Apollo (7324/2-1) and Atlantis (7325/1-1) had Jurassic and/or Triassic reservoir units as targets (NPD, 2017) and were drilled outside the Lower Cretaceous anomaly (Fig. 2a). Therefore, Ceres remains untested by drilling.

3. Data and method

3.1 Seismic and well data

In this study, we used a combination of 3D and wide-azimuth 2D high-resolution P-Cable seismic data acquired in 2014 and 2015. The P-Cable data coverage in the Hoop area is depicted in Fig. 1. P-Cable data have a typical frequency range of 8 to 270 Hz at -20dB, a very high near-offset trace density (3-6 meters native bin size) and a uniform traced distribution in both in-line and cross-line directions. The system provides unparalleled high-resolution seismic imaging, in the range of 3-7 meters vertically and up to 150 meters horizontally (Bellwald and Planke, in press; Crutchley et al., 2012; Plaza-Faverola et al., 2011). The horizontal and vertical resolutions of the P-Cable data are up to four times higher than conventional 3D seismic data. As illustrated in Fig. 5, P-Cable data is able to resolve two scales of clinoforms within the subaqueous delta NW2. On the other hand, the lack of far offsets in P-Cable data limits the potential for quantitative interpretation.

In addition, regional 2D seismic data acquired between 2006 and 2014 by TGS and Fugro are used to tie this study with the adjacent Fingerdjupet Subbasin. The exploration wells included in this study are 7324/2-1 (Apollo), 7325/1-1 (Atlantis) in the Hoop area and 7321/7-1 in the Fingerdjupet Subbasin (Fig. 1). The exploration wells on the Bjarmeland Platform are intersected by 2D P-Cable lines, whereas the well in the Fingerdjupet Subbasin is covered by regional 2D seismic data. We use available biostratigraphic information from well 7324/2-1 and 7321/7-1 (Robertson Group, 1989).

3.2 Seismic interpretation

Horizons were picked based on publicly available lithostratigrahic tops and are time-correlated in the Hoop area using the biostratigraphic information from well 7324/2-1. 2D seismic interpretation was performed in IHS Kingdom Suite, whereas we used Petrel for 3D seismic interpretation and attribute generation. In the Fingerdjupet Subbasin, the main seismic

reflections were time-correlated using biostratigraphic data from well 7231/7-1 (Fig. 1) and we followed the tectonostratigraphic framework established by Serck et al. (2017). In well 7321/7-1, not all the ages are based on direct biostratigraphic evidence (Serck et al., 2017), leading to some uncertainty in the horizon ages investigated in this work.

An example of interpreted high-resolution line going along the prograding direction of Lobe NW2 is shown in Fig. 5. BCU is a strong, continuous and hard reflection (i.e. a positive acoustic impedance contrast). Top Knurr is a weak reflection and was challenging to pick moving SW towards the Fingerdjupet Subbasin. Top Kolje is a hard reflection (Faleide, 2017), defined in previous work as a flooding surface linked to the delta Lobe NW2 (Hinna, 2016; Grundvåg et al., 2017). In places, Top Kolje is truncated by URU (Fig. 5), picked as a hard event corresponding to the base of the Quaternary sediments.

4. Results

4.1 Ceres in 2D conventional seismic data

We have mapped Ceres in 2D seismic data, defined as a bright anomalous event within the Lower Cretaceous succession, so the full outline of this spectacular elongated feature can be depicted on the lobe front map (Fig. 4). Ceres extends well beyond the sub-area shown in Fig. 2a, and the full length of the elongated anomaly is estimated to ~150 km, extending from the western Bjarmeland Platform to the SE edge of the Fingerdjupet Subbasin and nearby the present-day Loppa High (Fig. 1). The anomaly is as narrow as ~1 km to the NE and gradually widens up to ~8 km towards SW.

In Fig. 6, two examples of representative 2D conventional seismic lines are shown with the intention to place Ceres, the elongated bright event, in the stratigraphy of the Hoop area and the Fingerdjupet Subbasin. For a thorough tectono-stratigrahic analysis of the Fingerdjupet Subbasin, the reader is referred to Hinna (2016) and Serck et al. (2017). In Fig. 6, we interpreted the picks and establish a chronostratigraphic framework based on Serck et al. (2017). The color code defined in Fig. 6 indicates the interpreted age of each seismic facies and will be used throughout this contribution.

Interpretation of 3D/2D conventional seismic data has allowed to map the bright spot along the Barremian delta lobe front NW2 in the Kolje Formation. The Barremian prograding

lobe NW2 with oblique to sigmoidal clinoforms (Helland-Hansen and Hampson, 2009; Hinna, 2016) downlapping onto Top Knurr, was mapped using 2D conventional lines (Fig. 6) and 3D seismic data (Faleide, 2017). The termination of lobe NW2 is depicted in Fig. 4.

In Fig. 6b, Ceres is overlain by wedge-shaped, syn-rift strata (Hinna, 2016; Serck et al., 2017) forming the uppermost sequence of the Kolje Formation in the Fingerdjupet Subbasin. In Fig. 6a, the Top Kolje horizon is truncated by URU at the transition between the subbasin and the platform area, making the stratigraphic correlation challenging. However, biostratigraphic analysis of 7324/2-1 and seismic mapping indicate that a thin Barremian unit, attached to NW2, is directly overlain by Albian sediments of the Kolmule Formation in the Hoop area. Ceres is therefore overlain by Albian strata in the Hoop area (Fig. 6a). We subsequently note the absence of Aptian sediments, in particular the syn-rift strata of the subbasin, in the Hoop area and the subsequent draping of the whole area in Albian (Fig. 6).

4.2 High-resolution seismic facies

In this paragraph, the high-resolution seismic facies related to the elongated geophysical anomaly are investigated. Fig. 7a shows a high-resolution 3D seismic section through Ceres located at the transition between the platform area and the subbasin (Fig. 1). The principal axis of Ceres is roughly NE-SW (Fig. 7b). While the main stratigraphic units are identified on conventional 2D seismic data interpretation (Fig. 6), P-Cable seismic data display internal reflections within each seismic facies (Fig. 7a). In the Barremian unit, sigmoid to oblique clinoforms from NW2 are downlapping onto Top Knurr, the uppermost bound of the Early Barremian - Tithonian sequence (Hinna, 2016). As expected, Ceres stands out as a prominent isolated bright event on the P-Cable data. Some weak conformable reflections can be observed within the bright "lens". The top of Ceres is a soft event whereas the base is defined as a hard reflection. As observed previously in the Fingerdjupet Subbasin (Fig. 6a), Ceres lies at the base of the Aptian strata. This uppermost sequence of the Kolje Formation displays conformable, sometimes wavy, seismic reflections with an aggrading pattern. The same two-fold division of the Kolje Formation is described in Serck et al. (2017). We observe that these reflections onlap onto the top of the Barremian prograding unit NW2, denoted "iB" (Intra Barremian) in Serck et al. (2017) (Fig. 6a). This intra-Kolje unconformity truncates the underlying clinoforms from NW2, thereby representing an erosional surface (Fig. 7a). In the Kolmule Formation, reflections apparently onlap onto Top Kolje, the upper bound for the Aptian strata. We have computed the isopach map of Ceres (Fig. 7b) to try and restore its architecture. The isopach map (Fig. 7b) shows a ~5 km wide U-shape morphology, with a deeper, 2-3 km wide incision at its base. Its time-thickness ranges from 0 to ~20 ms. The feature has an asymmetric geometry: its northernmost flank has an abrupt termination while the other flank is gently pinching-out. Stratigraphically, Ceres was deposited on top of an erosive unconformity, denoted "iB" (Intra Barremian) in Serck et al. (2017).

Moving north, Fig. 8 displays a section and interpreted surface of a high-resolution 3D seismic survey intersecting Ceres in the Hoop area (Figs. 1 and 4). The seismic section shows the prograding Barremian lobe NW2 pinching-out, with clinoform downlapping onto Top Knurr. Contrarily to Fig. 7, we observe the presence of a distal unit at the bottomset of NW2 in Fig. 8. This unit, denoted NW2x, is a distal extension of lobe NW2 and displays conformable reflections that are parallel to Top Knurr and BCU horizons. Biostratigraphic analysis and available well tops from 7324/2-1 support that the Barremian distal unit NW2x is directly overlain by Albian sediments of the Kolmule Formation (Fig. 6a). Here, Ceres is part of the youngest sequence in the Kolje Formation and the top of the bright seismic event corresponds to the Top Kolje horizon. Ceres is conformably overlain by Albian-age strata with reflections onlapping onto NW2. A gradual upward evolution from layered-parallel reflection to a transparent seismic character in the Albian strata of the Kolmule Formation can be observed in the high-resolution data (Fig. 8a). Ceres shows pronounced internal layering. Similarly to Fig. 7a, Ceres displays an erosive base that truncates reflection of the underlying Barremian unit. The isopach map of Ceres (Fig. 8b) shows an asymmetric ~6 km wide U-shape geometry with a NE-SW principal axis. The maximal thickness of the geobody is 20 ms. In addition, we observe series of concentric arches in the isopach map, with a roughly ~100 meters separation (Fig. 8b). Some arches seemingly override each other. Furthermore, several Direct Hydrocarbon Indicators (DHI), i.e. a seismic attribute or pattern that could be explained by the presence of hydrocarbons, can be seen in P-Cable data. For example, a flat spot, i.e. a horizontal reflection cutting across beddings possibly representing the interface between Gas- and brine-filled sediments, and an amplitude brightening, are observed in the Stø Formation, along the westernmost fault (Fig. 8a).

Fig. 9 shows three high-resolution 2D seismic transects through Ceres in the Hoop area (Location in Fig. 4). In Fig. 9a, the line intersects well 7324/2-1 (Apollo), where formation tops are available (NPD, 2017). The same seismic facies described in Fig. 8a are present. However, the internal characteristics of Ceres evolve. The upper internal unit has a semi-transparent character, and overlays a very high-amplitude ~3 km wide layer at its erosive base. The bright unit pinches-out on each ends. The brightening was already observed in the RMS attribute map from 3D conventional seismic data and CSEM data suggests that the bright spot coincides with a resistive anomaly (Fig. 2; Baltar and Barker, 2017; Fanavoll et al., 2014). Note that Ceres is almost eroding down into Top Knurr (Fig. 9a). The Albian strata overlying Ceres consist of aggrading reflections onlapping onto Top Kolje. Still, a marked boundary from a layered to a reflection-free unit is readily observed within the Albian-age Kolmule Formation (Fig. 9).

The development of a thicker distal unit at the bottomset of NW2 is remarkable. This distal toeset (NW2x; Fig. 9b) of the Barremian unit thickens from ~20 meters (Fig. 9a) to ~60 meters (Fig. 9b) according to publicly available well tops (NPD, 2017) and Faleide (2017). Ceres is thinner and seemingly divided into two incisions. High-amplitude conformable reflections in Lower Albian onlap onto Top Kolje to the North.

We observe the easternmost evidence of an erosional truncation into the Barremian clinoforms (NW2) in high-resolution seismic data in Fig. 9c. The soft kick, i.e. negative amplitude anomaly, has vanished at the erosive base. Instead, three ~1 km-wide incisions, one with a V-shape morphology to the west and two U-shaped towards NE, carve into the prograding unit NW2. The westernmost incision displays a prograded infill pattern. The middle incision display a vertical stacking pattern.

5. Discussion

5.1 Summary of results

Using a combination of 3D, wide-azimuth 2D high-resolution and conventional seismic data, we have described in detail an enigmatic ~150 km long, high amplitude, resistive anomaly in the Hoop area, terminating at the southeastern edge of the Fingerdjupet Subbasin (Fig. 4). The elongated-shape feature is following the contour of a subaqueous delta lobe NW2. High-resolution seismic data reveal that Ceres is the basal unit of an Aptian sequence resting on a hard, erosional surface not visible on conventional seismic data (Fig. 2b). A single 6 km wide, U-shaped incision to the west, separating in three 1-km V-shaped incisions to the east of the study area. In the following, we propose and discuss an evolutionary model for a submarine slope channel system in the Hoop area. In an attempt to place the study in the regional context of the SW Barents Sea, we then produce a paleo-geographic reconstruction of the study area at a key stage of the formation of Ceres. The final part of the discussion is concerned with the implications for petroleum prospectivity.

5.2 Evolutionary model of Ceres

Based on the seismic observations, we propose an evolutionary model of a diverted submarine channel in the Hoop area in four stages (Fig. 10).

Stage I: Arrival of subaqueous delta NW2 - Barremian (Fig. 10a)

At the onset of High Arctic Large Igneous Province magmatism (HALIP; Senger et al., 2014; Polteau et al., 2016), crustal doming to the NW of present-day Svalbard triggered the widespread and stable progradation of sedimentary units to offshore areas (Midtkandal and Nystuen, 2009; Grundvåg et al., 2017). In Barremian, subaqueous delta NW2 has prograded up to the Hoop area but the lobe front extends hundreds of kilometers, from the Fingerdjupet Subbasin to the central Bjarmeland Platform (Figs. 4 and 5). In addition, we interpret the presence of a distal unit (NW2x) attached to the subaqueous delta (NW2) in the Hoop area (Figs

8a, 9a and 9b). This unit has been described by Dimitriou (2014) as the extended toeset of NW2. We propose that these pro-delta deposits, denoted NW2x, may have formed as a deceleration sheet or pro-delta plume. Atlantis and Apollo have penetrated ~60 meters and ~20 meters, respectively, of this marine mudstone-dominated (NPD, 2017) distal wedge. The top of the prograding unit is a regional flooding surface. Denoted "iB" (Intra Barremian), this horizon was assigned a Late Barremian – Early Aptian age in Serck et al. (2017) (Fig. 6) whereas Grundvåg et al. (2017) place the flooding surface well into mid-Aptian. These contradicting observations reflect the uncertainty of the biostratigraphy analysis in well 7321/7-1. Consequently, the term "iB" (Intra Barremian) used in Serck et al. (2017) is misleading as "iB" is most likely Aptian age.

Stage II: Sea level rise, sediment starvation and submarine erosion - Aptian (Fig. 10b)

At this stage, the Barents Shelf recorded an episode of uplift to the NE (Grundvåg et al., 2017). This event led to the shift of the paleo-drainage system and lobe progradation direction from NW-SE (NW1 and NW2) to NE-SW (NE1, NE2, NE3) and a marked sea-level rise (Midtkandal et al., 2016). This uplift episode combined with the onset the North Atlantic rifting, is reflected by an increased subsidence rate and vertical settling of sediments in the Fingerdjupet Subbasin in the Aptian Stage. Meanwhile, the NW-sourced lobes were flooded and replaced by an open-marine environment (Grundvåg et al., 2017; Marín et al., 2017). The Hoop area was lying on sediment-starved slopes, which is supported by the absence of Aptian sediments (Figs. 8 and 9). A dramatic thickening of the Aptian strata has been reported in the SE edge of the Fingerdjupet Subbasin (Fig. 4.2 in Hinna (2016)) that we interpret as an embayment toward the deep Bjørnøya Basin (Fig. 1). The Fingerdjupet Subbasin was undergoing an episode of extension where outer to deep shelfal conditions prevailed (Smelror et al., 2009). We claim that bottom currents, flowing E-W, carved a major submarine channel system on the tilted slopes of the Hoop area, terminating in a sediment sink to the SE edge of the Fingerdjupet Subbasin.

This interpretation supports that the course of the submarine channel was obstructed by the relict-topography of NW2 lobe front (Figs. 4 and 5), diverting its natural downslope pathways and thus explaining why the principal channel mimics the concave shape of the delta front. The steep foresets of a subaqueous delta NW2 acted as a seafloor obstacle, funneling contour-parallel currents (Rebesco et al., 2014) and therefore carving a channel parallel to NW2 front in the Hoop area. Ceres could have then served as a fairway for easterly sediments feeding the SE Fingerdjupet Subbasin and deep Bjørnøya Basin in Aptian. We suspect that bottom currents were also diverted by the nearby Loppa High and Svalis Dome, both being uplifted topographic highs (Indrevær et al., 2016).

Submarine channels are known to have their courses diverted by tectonic activity and/or seafloor topography such as salt domes (Gamboa et al., 2012; Rebesco et al., 2014; Zucker et al., 2017) but, to our knowledge, there is no documented examples of channel systems diverted by pre-existing subaqueous delta lobe fronts. Clark et al. (2009) proposes a classification of key submarine channel-structure interaction and the Ceres channel – delta lobe NW2 illustrates undoubtedly a "diversion". In addition, isopach map (Figs. 7b and 8b) show that Ceres is characterized by low sinuosity in the Hoop area. The series of semi-circular ridges observed in Fig. 8b could arguably represent relict sediment waves (Lee et al., 2002; Wynn et al., 2002) generated by NE-SW paleo-flows within the main channel.

A straight channel course with no apparent meanders is interpreted in the available database. This linear geometry supports relatively steep seabed slopes in the Aptian Hoop area as channel sinuosity is generally inversely proportional to slope gradient (Slatt, 2013).

In two high-resolution seismic sections, the most proximal part of Ceres includes several tributaries, comprising up to three separate and 1-3 km wide V-shaped incisions (Fig. 9b and 9c). The tributaries seemingly merges into a ~8-km wide U-shaped principal channel in the Hoop area (Figs. 8 and 9c) and at the transition to the subbasin (Fig. 7). Present-day and buried

submarine canyons often exhibit narrow, deep V-shaped incisions (Harishidayat et al., 2018; Jobe et al., 2010; Ferry et al., 2004). The strong negative amplitude event (Figs. 5, 7, 8, 9a and 9b) represents a sedimentary unit deposited during the early infilling phase of Ceres. Based on analogue environments, reworked, coarser-grained sediments deposited at the erosive base of submarine canyon often respond with a negative-amplitude signature in seismic data (Ferry et al., 2004; Jobe et al., 2010). We report the presence of NE-SW prograding units, named NE1, NE2 and NE3, on the Bjarmeland Platform with ages spanning from Aptian to Albian based on analysis of dense grid of regional 2D lines tied to several wells in the SW Barents Sea. With the current seismic coverage and due to severe erosion of Early Cretaceous strata in the Bjarmeland Platform, it is challenging to relate the submarine channel to either NE2 or NE3 and their shelf break in the study area (Fig. 4).

Evidences listed in this paragraph allow to speculate on the existence of a Contourite Depositional System (CDS) (Rebesco et al., 2014 and reference therein) with Ceres acting as an alongslope channel and sediment fairway leading to a sink at the SE corner of the Fingerdjupet Subbasin.

Stage III: Hemipelagic deposition and passive infill of Ceres – Early Albian (Fig. 10c)

The absence of Aptian sediments in the Hoop area (except for the active in-filling in Ceres) supports that the zone was already uplifted relatively to the Fingerdjupet Subbasin (Fig. 6). At this stage, hemipelagic rain deposition occurred exclusively in a well-bounded, rapidly subsiding Fingerdjupet Subbasin (Hinna, 2016; Figs 6, 7 and 8). Hemipelagic sediment deposition reached the platform area in Albian (Fig. 6a). Onlapping reflections onto the Top Kolje horizon on both Fingerdjupet Subbasin (Figs. 6 and 7) and Hoop area (Figs. 8 and 9) illustrate this model and shows that a structural high potentially separated these two depocenters (Fig. 6a). At this stage, the Ceres submarine channel system was abandoned and passive infill of the incision with marine muds occurred in the Hoop area (Fig. 9c).

Stage IV: Arrival of NE-sourced lobe, mud draping - Albian (Fig. 10d)

During Albian, a sedimentary unit draped both the Fingerdjupet and Hoop areas (Fig. 6a; Serck et al., 2017). A change in seismic character (Figs. 8 and 9) from high amplitude reflections to a transparent, reflection-free unit indicates a sharp variation in lithology. The easterly sedimentary lobe NE1 draped the Hoop area in Albian and most likely the adjacent Fingerdjupet (Figs. 6, 8 and 9). A growth sequence in Albian strata is reported by Faleide (2017) in the Hoop area (Fig. 1). In Fig. 8a, normal faults are activated after the Aptian channel erosion. As a result, the Albian tectonic quiescence in the Fingerdjupet Subbasin discussed in Serck et al. (2017) may not apply to the Hoop area. If a new period of tectonic activity occurred in Albian in the Hoop area is beyond the scope of this study.

5.3 Paleo-geographic reconstruction

We have reconstructed the paleo-geography of a sub-region of the SW Barents Sea at the Aptian stage, from the North of Loppa High to the south of Bear Island (Fig. 11). The reconstruction is based on the interpretation of the prograding units (Fig. 4) and Ceres (Fig. 10b), as well as collating the paleo-environment of the northern Loppa High described in Marín et al. (2018) and Harishidayat et al. (2018). The Aptian reconstruction in Fig. 11 reveals a smoothly-varying submarine topography to the north and east of the study area, shaped by sedimentary lobes (Fig. 4), contrasting with a highly-structured, steep slopes along the emerging Loppa High and Svalis Dome to the south (Marín et al., 2018). The map also highlights an oceanographic aspect by depicting paleo-currents and associated sediments drainage. Turbulent slope currents were dominant on the steep slopes of the western Loppa High, carving submarine canyons and forming short-length turbidite fan systems confined by normal faults (Marín et al., 2018). On the contrary, the tectonically-quiet Bjarmeland Platform display a long-distance submarine drainage pattern, Ceres. There, bottom currents were funneled at the toeset of a flooded delta lobe NW2 forming a 220-290 meters bathymetric

obstacle in Aptian (Figs. 4, 5 and 10b). To our knowledge, this study is the first to propose the formation of a diverted submarine channel along a pre-existing subaqueous delta lobe front, obstructing its flow pathway. The easterly sediments were subsequently drained through Ceres and accumulated in a depocenter, located to the southeastern corner of the Fingerdjupet Subbasin (Fig. 11; Hinna, 2016). The narrow "strait" between the bathymetric high formed by NW2 and the Svalis Dome was arguably the locus of major water outflow (Fig. 11), discharging large amounts of NE-sourced sediments to the subsiding Bjørnøya Basin, at the onset of the North Atlantic rifting.

5.4 Implications for petroleum prospectivity

Integration of CSEM and seismic data for prospect de-risking has proven a successful strategy in the Hoop area. Recent hydrocarbon discoveries Wisting (7324/8-1), Hanssen (7324/7-2), Mercury (7324/9-1) and Gemini North (7325/4-1) in good quality reservoir sands of the Jurassic-Late Triassic Realgrunnen Subgroup were systematically associated with coincident highly resistive anomalies and seismic DHIs (Alvarez et al., 2018; Baltar and Barker, 2017; Granli et al., 2017). The size of Gemini North discovery (7325/4-1) is inferior to 6 million barrels of oil equivalent and illustrates the high sensitivity of the CSEM method to sub-commercial, shallow-buried hydrocarbon accumulations in the Hoop area. Although originating from the Lower Cretaceous interval, Ceres also displays a coincident high acoustic amplitude, resistive anomaly (Fig. 2). The interpretation of Ceres as an Aptian submarine channel system increases the probability of presence of reworked sands, deposited along the erosive base of the submarine channel (Figs. 7, 8 and 9). Moreover, the juxtaposition of the Aptian channel and Stø Formation along normal faults, activated in Albian (Fig. 8a) suggests that hydrocarbons may migrate from the prolific Stø Formation. Therefore Ceres could be a stratigraphic trap,

faulted in places, with high-porosity sandstones saturated with hydrocarbons, and thereby explaining the elongated seismic amplitude and resistive anomalies along NW2 (Fig. 2).

However, high resistivity in sedimentary basins can be caused by several type of lithologies such as basalt, salt, cemented sandstone, carbonate and source rock (Baltar and Barker, 2015). Nevertheless, the depositional environment of the Early Cretaceous Barents (Fig. 11; Grundvåg et al., 2017) and seismic signature allows to discard volcanic rocks, salt, cemented sandstones and tight carbonates.

In the following paragraph, we investigate a second plausible interpretation for Ceres as a mature, organic-rich source rock. This alternative explanation is supported by the presence of source rock in exploration well 7321/9-1 in the adjacent Fingerdjupet Subbasin (Fig. 1). This source rock of high-organic content is penetrated in the Aptian sequence forming the upper part of the Kolje Formation (Hinna, 2016), from 961 to 986 meters below mudline (Robertson Group, 1989). Borehole data shows deep resistivity peaking at ~17 Ω.m in the source rock, four times higher than the average 4-5 Ω.m background value recorded in the Kolmule and Kolje Formations (NPD, 2017). Even though we interpret the end of the Aptian channel in the vicinity of the well (Fig. 4), we cannot exclude that with a better seismic data coverage Ceres would extend further into the subbasin (Fig. 11). The two nearby wells (7321/8-1 and 7321/7-1) drilled on local highs, do not show traces of source rock in the Kolje Formation (NPD), thereby illustrating the complex distribution of the Aptian source rock in the Fingerdjupet Subbasin. On the opposite side of the Loppa High (Fig. 1), in the Hammerfest Basin, well 7122/2-1 penetrates two intervals of organic-rich source rock. Borehole data shows a 15-meters thick source rock in the Kolje Formation (NPD), with deep resistivity log values averaging ~15 Ω.m over the interval and a 82-meters thick source rock, the Hekkingen Formation, averaging ~50 Ω.m over the interval, with resistivity values reaching up to 100 Ω.m. Well 7122/2-1 shows that Hekkingen Formation source rock could potentially reach high ATR

values (Baltar and Barker, 2015), and explain the resistive anomaly retrieved from CSEM data in Ceres (Fig. 2; Baltar and Barker, 2017). Senger et al. (2017) investigate resistivity variations in exploration boreholes in the Barents Sea and crucially conclude that resistivity of organic-rich shales of the Hekkingen Formation is a function of total organic content and maturation level. Extrapolating the latter conclusion to the source rock of the Kolje formation, we infer that if Ceres is an Aptian source rock then it has reached a mature stage in the Hoop area given its high resistivity (Fig. 2).

We favor the hydrocarbon-bearing scenario as high resistivity anomaly in CSEM data could not account for intermediate resistivity values of ~15 Ω.m recorded in the 25-meter thick, Aptian source rock in well 7321/9-1. Nevertheless, we expect that both scenarios, (1) hydrocarbon accumulation in a faulted stratigraphic trap, and (2) mature source rock with high-organic content confined to a submarine channel, would have a significant impact on exploration strategies in the SW Barents Sea.

6. Conclusion

The elongated seismic amplitude and resistive response of Aptian sediments deposited on the erosive base of the submarine channel has attracted the interest of oil and gas explorers in the SW Barents Sea. Geophysical and geological evidences points toward the development of a submarine channel system in Aptian in the Hoop area and terminating in a depocenter located at the SE edge of the Fingerdjupet Subbasin. A specificity of this submarine channel, named Ceres, lies in its close relationship with an older subaqueous delta front. The relict-topography of a flooded NW-sourced delta has funneled bottom currents along its toeset to carve a contouritic channel. To our knowledge, this contribution is the first to document a submarine channel course diverted by a pre-existing subaqueous delta lobe. This important observation is illustrated in a paleo-geographic reconstruction of the SW Barents Sea. We also conclude that the Ceres submarine channel forms a stratigraphic trap holding hydrocarbon-

bearing sandstones or alternatively contains a mature, organic-rich source rock of easterly provenance. Both hypothesis have important implications for petroleum prospectivity and/or distribution of a mature, organic-rich Aptian source rock in the southwestern Barents Sea.

Acknowledgements

The authors wish to thank VBPR, TGS, WGP Survey and Spectrum for allowing to publish their multiclient data. Stéphane Polteau is thanked for review and comments that helped improve the clarity of the manuscript. VBPR geologist Benjamin Bellwald and Amer Hafeez are acknowledged for stimulating discussions and comments. Finally, we would like to thank Stein Fanavoll and Reidar Müller for discussions and useful insights on the subject of this work. Alf Ryseth is acknowledged for biostratigraphic informations, providing important constrains on the interpretation. J.I Faleide and S. Planke acknowledge support from the Research Council of Norway through its Centers of Excellence funding scheme, Project Number 223272. We thank Kim Senger and an anonymous reviewer for constructive remarks that helped improve the quality of the manuscript.

References

Allen, P., and Allen L.R., 1990. Basin analysis. Principles and applications: Oxford, Blackwell Scientific Publications, p. 451. https://doi.org/10.1016/j.marpetgeo.2016.02.024

Alvarez, P., Marcy, F., Vrijlandt, M., Skinnemoen, Ø., MacGregor, L., Nichols, K., Keirstead, R., Bolivar, F., *et al.* 2018. Multi-physics characterisation of reservoir prospects in the Hoop area of the Barents Sea. *Interpretation*, **6**, 1-51 https://doi.org/10.1190/int-2017-0178.1

Århus, N., 1991. The transition from deposition of condensed carbonates to dark claystones in the Lower Cretaceous succession of the southwestern Barents Sea. Norsk Geologisk Tidsskrift 71, p. 259-263. ISSN 0029-196X

Baig, I., Faleide, J.I., Jahren, J., Mondol, N.H., 2016. Cenozoic exhumation on the southwestern Barents shelf: Estimates and uncertainties constrained from compaction and thermal maturity. Marine and Petroleum Geology v73, p.105-130. https://doi.org/10.1016/j.marpetgeo.2016.02.024

Baltar, D., Barker, N., 2017. Reservoir quality prediction with CSEM. First Break, v. 35/9, p. 48-53

Baltar, D., Barker, N., 2015, Prospectivity Evaluation with 3D CSEM. First Break, v. 33/9, p. 55-62

Baltar, D., Roth, F., 2013, Reserves Estimation Methods for Prospect Evaluation with 3D CSEM Data. First Break, v. 31, p. 103-111.

Bellwald, B., Planke, S., Piasecka, E.D., Matar, M.A., Andreassen, K., in press. Ice-stream dynamics of the SW Barents Sea revealed by high-resolution 3D seismic imaging of glacial deposits in the Hoop area. Marine Geology. https://doi.org/10.1016/j.margeo.2018.03.002

Bellwald, B., Planke, S., in press. Shear Margin Moraine, Mass Transport Deposits, and Soft Beds Revealed by High-Resolution P-Cable 3D Seismic Data in the Hoop Area, Barents Sea. Geological Society of London. https://doi.org/10.1144/SP477.29

Binns, P.E, 2006. Evaluating subtle stratigraphic traps: prospect to portofolio. Geological Society, London, Special Publications, 254, p. 7-26. https://doi.org/10.1144/GSL.SP.2006.254.01.02

Carstens, H., 2014. De tre skuffelsene. Online article: www.geo365.no/olje-og-gass/de-tre-skuffelsene

Clark, I.R, Cartwright, J.A., 2009. Interactions between submarine channel systems and deformation in deepwater fold belts: Examples from the Levant Basin, Eastern Meditteranean Sea. Marine and Petroleum Geology v. 26, p. 1465-1482. doi:10.1016/j.marpetgeo.2009.05.004

Constable, S., and C.J. Weiss, 2006, Mapping Thin Resistors and Hydrocarbons with Marine EM Methods: Insights from 1D Modeling. Geophysics, v. 71/2, p. 43-51. https://doi.org/10.1190/1.2187748

Crutchley, G.J., Karstens, J., Berndt, C., Talling, P.J., Watt, S.F.L., Vardy, M.E., Hühnerbach, V., Urlaub, M., Sarkar, S., Klaeschen, D., Paulatto, M., Le Friant, A., Lebas, E., Maeno, F., 2012. Insights into the emplacement dynamics of volcanic landslides from high-resolution 3D seismic data acquired offshore Montserrat, Lesser Antilles. Marine Geology 335, 1-15. https://doi.org/10.1016/j.margeo.2012.10.004

Dimakis, P., Braathen, B.I., Faleide, J.I., Elverhoi, A., Gudlaugsson, S.T., 1998. Cenozoic Erosion and the Preglacial Uplift of the Svalbard-Barents Sea Region. Tectonophysics 300, p. 311-327. https://doi.org/10.1016/S0040-1951(98)00245-5

Dimitriou, M., 2014. Lower Cretaceous Prograding Units in the eastern part of the SW Barents Sea. Master thesis, University of Oslo. http://urn.nb.no/URN:NBN:no-46690

Eidesmo, T., S. Ellingsrud, L.M. MacGregor, S. Constable, M.C. Sinha, S. Johansen, F.N. Kong, Westerdahl, H., 2002. Sea Bed Logging (SBL), A New Method for Remote and Direct Identification of Hydrocarbon Filled Layers in Deepwater Areas. First Break, v. 20, p. 144-152.

Faleide, J.I., Vågnes, E., Gudlaugsson, S.T., 1993. Late Mesozoic-Cenozoic evolution of the south-western Barents Sea in a regional rift-shear tectonic setting. Marine and Petroleum Geology v10, p.186-214. https://doi.org/10.1016/0264-8172(93)90104-Z

Faleide, T.S., 2017. High-resolution 3D seismic interpretation of a Lower Cretaceous delta system in the Hoop area, SW Barents Sea. Master Thesis, University of Oslo. http://urn.nb.no/URN:NBN:no-60752

Fanavoll, S., Gabrielsen, P. and Ellingsrud, S., 2014. CSEM as a tool for better exploration decisions: Case studies from the Barents Sea, Norwegian Continental Shelf. Interpretation, Vol. 2, No. 3, p. 55-6. http://dx.doi.org/10.1190/INT-2013-0171.1

Ferry, J-N., Babonneau, N., Mulder, T., Parize, O. and Raillard, S., 2004. Morphogenesis of Congo submarine canyon and valley: implications about the theories of the canyons formation, Geodinamica Acta, 17:4, 241-251, DOI: 10.3166/ga.17.241-251

Gabrielsen, R.H., Færseth, R.B., Jensen, L.N., Kalheim, J.E., Riis, F., 1990. Structural elements of the Norwegian continental shelf. Part I: The Barents Sea Region. In: NPD-Bulletin no 6. ISBN 82-7257-304-0

Gamboa, D., Alves, T.A. and Cartwright, J., 2012. A submarine channel confluence classification for topographically confined slopes. Marine and Petroleum Geology v35, p. 179-189. doi:10.1016/j.marpetgeo.2012.02.011

Granli, J.R., Veire, H.H., Gabrielsen, P. & Morten, J.P. 2017. Maturing broadband 3D CSEM for improved reservoir property prediction in the Realgrunnen Group at Wisting, Barents Sea *SEG Technical Program Expanded Abstracts 2017*. Society of Exploration Geophysicists, 2205-2209. https://doi.org/10.1190/segam2017-17727091.1

Green, P.F., Duddy, I.R., 2010. Synchronous exhumation events around the Arctic including examples from Barents Sea and Alaska North Slope, in: Vining, B.A., Pickering, S.C. (Eds.), Petroleum Geology: from Mature Basins to New Frontiers-Proceedings of the 7th Petroleum Geology Conference, p. 633-644. https://doi.org/10.1144/0070633

Grundvåg, S.-A., Marin, D., Kairanov, B., Śliwińska, K.K., Nøhr-Hansen, H., Escalona, A., Olaussen, S., 2017. The Lower Cretaceous succession of the northwestern Barents Shelf: Onshore and offshore correlations. Marine and Petroleum Geology v86, p. 834-857. DOI: 10.1016/j.marpetgeo.2017.06.036.

Gudlaugsson, S.T., Faleide, J.I., Johansen, S.E., Breivik, A.J., 1998. Late Palaeozoicstructural development of the south-western Barents Sea. Marine and Petroleum Geology v15, p.73-102. http://dx.doi.org/10.1016/S0264-8172(97)00048-2.

Harishidayat, D., Omosanya, K.O., Johansen, S.E., Eruteya, O.E., Niyazi, Y. 2018. Morphometric analysis of sediment conduits on a bathymetric high: implications for plaeoenvironment and hydrocarbon prospectivity. Basin research. In press. https://doi.org/10.1111/bre.12291

Helland-Hansen, W., Hampson, G.J., 2009. Trajectory analysis: concepts and applications. Basin Research 21, p. 454-483. DOI: 10.1111/j.1365-2117.2009.00425.x

Henriksen, E., Bjørnseth, H.M., Hals, T.K., Heide, T., Kiryukhina, T., Kløvjan, O.S., Larssen, G.B., Ryseth, A.E., Rønning, K., Sollid, K., Stoupakova, A., 2011b. Uplift and erosion of the greater Barents Sea: impact on prospectivity and petroleum systems, in: Spencer,

A.M., Embry, A.F., Gautier, D.L., Stoupakova, A.V., Sørensen, K. (Eds.), Arctic Petroleum Geology, Geol. Soc. London, 35, p. 271-281. https://doi.org/10.1144/M35.17

Hinna, C.H., 2016. Seismic characterization of Lower Cretaceous Clinoform packages in the Fingerdjupet Subbasin, Southwestern Barents Sea. Master Thesis, Faculty of Science and Technology, the University of Stavanger. http://hdl.handle.net/11250/2414770

Indrevær, K., Gabrielsen, R.H., and Faleide, J.I., 2016. Early Cretaceous syn-rift uplift and tectonic inversion in the Loppa High Area, southwestern Barents Sea, Norwegian shelf. Journal of the Geological Society. p. 174-242. https://doi.org/10.1144/jgs2016-066

Indrevær, K., Gac, S., Gabrielsen, R.H., and Faleide, J.I., 2017. Crustal scale subsidence and uplift caused by metamorphic phase changes in the lower crust: A model for the evolution of the Loppa High area, SW Barents Sea from late Palaeozoic to Present. Journal of the Geological Society. Geological Society of London. https://doi.org/10.1144/jgs2017-063

Jobe, Z.R., Lowe, D.R. and Uchytil, S.J., 2010. Two fundamentally different types of submarine canyons along the continental margin of Equatorial Guinea. Marine and Petroleum Geology 28, p. 843-860. doi:10.1016/j.marpetgeo.2010.07.012

Laberg, J.S., Andreassen, K., Vorren, T.O., 2012. Late Cenozoic erosion of the high-latitude southwestern Barents Sea shelf revisited. GSA Bull. 124, 77-88. https://doi.org/10.1130/B30340.1

Lee, H.J., Syvitsky, J. P. M., Parker, G., Orange, D., Locat, J., Hutton, J. H. W., and Imran, J., 2002. Distinguishing sediment waves from slope failure deposits: field examples, including the "Humboldt Slide" and modelling results, Mar. Geol., 192, 79– 104.

Marín, D.,Escalona, A., Śliwińska, K.K.,Nohr-Hansen, H., and Mordasova, A., 2017. Sequence stratigraphy and lateral variability of Lower Cretaceous clinoforms in the SW Barents Sea. AAPG Bulletin, doi: 10.1306/10241616010

Marín, D., Escalona, A., Grundvåg, S-A., Nøhr-Hansen, H., Kairanov, B., 2018. Effects of adjacent fault systems on drainage patterns and evolution of uplifted rift shoulders: The Lower Cretaceous in the Loppa High, southwestern Barents Sea. Marine and Petroleum Geology, vol. 94, p. 212-229, https://doi.org/10.1016/j.marpetgeo.2018.04.009

Midtkandal, I., and Nystuen, J.P., 2009. Depositional architecture of a low-gradient ramp shelf in an epicontinental sea: The lower Cretaceous of Svalbard. Basin Res. 21, 655–675. doi:10.1111/j.1365-2117.2009.00399.x

Midtkandal, I., Faleide, J.I., Dahlberg, E., Dimitriou, M., Nystuen, J.P., 2014. The Lower Cretaceous strata in Svalbard and the Barents Sea: basin infill dynamics and paleobathymetry. Extended abstract. EGU General Assembly. May 2014, Vienna, Austria. 2014EGUGA..612638M

Midtkandal, I., et al., 2016. The Aptian (Early Cretaceous) oceanic anoxic event (OAE1a) in Svalbard, Barents Sea, and the absolute age of the Barremian-Aptian boundary. Palaeogeogr. Palaeoclimatol. Palaeoecol. DOI: 10.1016/j.palaeo.2016.09.023

NPD, 2017. Factpages of Exploration Wellbores [Online]. http://factpages.npd.no/factpages/

Plaza-Faverola, A., Bünz, S., Mienert, J., 2011. Repeated fluid expulsion through sub-seabed chimneys offshore Norway in response to glacial cycles. Earth and Planetary Science Letters 305, 297-308. https://doi.org/10.1016/j.epsl.2011.03.001

Polteau, S., Hendriks, B.W.H., Planke, S., Ganerød, M., Corfu, F., Faleide, J.I., Midtkandal, I., Svensen, H.S. and Myklebust, R., 2016. The Early Cretaceous Barents Sea Sill Complex: Distribution, $^{40}Ar/^{39}Ar$ geochronology, and implications for carbon gas formation.Palaeogeogr. Palaeoclimatol. Palaeoecol. DOI: 10.1016/j.palaeo.2015.07.007

Rebesco, M., Hernandez-Molina, F.J., Van Rooij, D., Wåhlin, A., 2014. Contourites and associated sediments controlled by deep-water circulation circulation processes: State-of-the-art and future considerations. Marine Geology, vol. 352, p. 111-154 http://dx.doi.org/10.1016/j.margeo.2014.03.011

Robertson Group, 1989. Mobil 7321/7-1 Norwegian Barents Sea Well: Biostratigraphy of the Interval 613m (SWC)-3552m (TD).

Sættem, J., Poole, D.A.R., Ellingsen, L., Sejrup, H.P., 1992. Glacial geology of outer Bjørnøyrenna, southwestern Barents Sea. Marine Geology 103, p. 15-51. https://doi.org/10.1016/0025-3227(92)90007-5

Senger, K., Tveranger, J., Ogata, K., Bråthen, A., Planke, S., 2014. Late Mesozoic magmatism in Svalbard: A review. Earth-Science Reviews 139. https://doi.org/10.1016/j.earscirev.2014.09.002

Senger, K., Birchall, T., Ohm, S., Olaussen, S., Ogata, K., 2017. Review of geological controls on resistivity in uplifted basins: insights from the Norwegian Barents Shelf. Extended Abstract. AAPG/SEG 2017 Internationl Conference and Exhibition, London, England. http://www.searchanddiscovery.com/pdfz/documents/2017/30535senger/ndx_senger.pdf.html

Serck, C.S., Faleide, J.I., Braathen, A., and Kjølhamar, B., 2017. Jurassic to Early Cretaceous basin configurations(s) in the Fingerdjupet Subbasin, SW Barents Sea. Marine and Petroleum Geology,v 86,p 874-891. http://dx.doi.org/10.1016/j.marpetgeo.2017.06.044

Slatt, R.S., 2013. Statigraphic Reservoir Characterization for Petroleum Geologists, Geophysicists, and Engineers, v. 61, 2nd edition. ISBN: 9780444563705

Smelror, M., Mørk, A., Monteil, E., Rutledge, D., and Leereveld, H., 1998. The Klippfisk Formation – a new lithostratigraphic unit of Lower Cretaceous platform in the Western Barents Shelf. Polar Research, v. 17. p. 181-202. doi:10.1111/j.1751-8369.1998.tb00271.x

Smelror, M.O., Petrov, Larssen, G.B., and Werner, S., 2009. Geological history of the Barents Sea: Norges Geol. undersøkelse, p. 1-135.

Wynn, R.B. and Stow D.A.V., 2002. Classification and characterization of deep-water sediment waves. Marine Geology 192, p. 7-22. doi:10.1016/S0025-3227(02)00547-9

Zucker, E., Gvirtzman, Z., Steinberg, J. and Enzel, Y., 2017. Diversion and morphology of submarine channels in response to regional slopes and localized salt tectonics, Levant Basin. Marine and Petroleum Geology, v. 81, p. 98-111. http://dx.doi.org/10.1016/j.marpetgeo.2017.01.002

Fig. 1 Seismic and well database used in this study overlaid on the structural elements map (NPD, 2017). The insert map on the bottom right corner shows the location of the study in the Barents Sea. HFC: Hoop Fault Complex; MH: Mercurius High.

Fig. 2 A NE-SW elongated high-amplitude and resistive anomaly originating from Lower Cretaceous in the Hoop area a) RMS amplitude map from 3D conventional seismic data (Modified from Faleide (2017); data courtesy of TGS). The RMS time window is defined between BCU and BCU + 110 ms. The outline of the resistive anomaly is depicted as a dashed white line and is extracted from Baltar and Barker (2017). The location of the map is shown in Fig. 1 b) 2D conventional seismic profile showing the Lower Cretaceous unit, focus of this work, is bounded by the red (URU), blue (BCU) horizons. The brown area depicts a prograding deltaic lobe and its clinoform surfaces. Profile location in Fig. 2a. BCU: Base Cretaceous Unconformity, URU: Upper Regional Unconformity

Fig. 3 Mid-Cretaceous – Upper Jurassic lithostratigraphic and seismic stratigraphic framework of the study area. The grey color represents mudstones with varying shale content and yellow represents sandstones (NPD, 2017). The seismic to well correlation for Atlantis (7325/1-1) and Apollo (7324/2-1) is displayed on high-resolution seismic data. BCU: Base Cretaceous Unconformity. URU: Upper Regional Unconformity. Chronostratigraphic chart modified from Midtkandal et al. (2016).

Fig. 4 Map of the prograding lobe front termination in the study area and overlain on the outline of Ceres, defined by the lateral extent of a prominent seismic anomaly (this study) and the main structural elements (NPD, 2017). The dashed part of the lines represent area where the lobe front interpretation is uncertain due to erosion and/or data coverage. Note how Ceres embraces the contour of the front of delta lobe NW2 in the Hoop area and terminates to the SE corner of the Fingerdjupet Subbasin. The dark blue lines stand for the seismic transects and surfaces displayed in this work. MB: Maud Basin; HFC: Hoop Fault Complex; MH: Mercurius High.

Fig. 5 Example of an interpreted high-resolution P-Cable 2D line through the Barremian prograding unit NW2. The BCU and URU horizon bound the stratigraphy of Early Cretaceous age (Fig. 3). Two scales of clinoforms with oblique to sigmoid geometries downlapping onto Top Knurr are resolved in the P-Cable data. The profile location is marked in Fig. 4.

Fig. 6 2D interpretation of Lower Cretaceous seismic horizons. a) Composite 2D conventional seismic profile showing the main stratigraphic units, horizons and structural elements of the study area; from E to W, the Hoop area of the Bjarmeland Platform and

Fingerdjupet Subbasin. The dashed vertical lines indicate a change in seismic line direction. b) 2D seismic profile showing the main stratigraphic units and horizons in the Fingerdjupet Subbasin. The profile location is provided in Fig. 4. The white solid line stand for clinoform surfaces of NW2. The nomenclature and interpretation established by Serck et al. (2017) is reproduced in this figure. Profiles located in Fig. 4. Seismic data courtesy of TGS and Spectrum.

Fig. 7 Interpretation of high-resolution seismic facies in a P-Cable 3D seismic survey adjacent to the Fingerdjupet Subbasin a) Uninterpreted (top) and interpreted (bottom) section in the SE corner of the Fingerdjupet Subbasin. The interpreted section shows the Lower Cretaceous horizons and the black solid lines highlights the beddings within each seismic facies. The red arrows indicate truncated reflections. The 3D survey location is provided in Fig. 4, and the profile location is depicted by the black solid line in Fig. 7b. b) Isopach map of Ceres, showing the U-shaped incision into the Barremian prograding unit. The major faults are depicted by white framed polygons.

Fig. 8 Interpretation of high-resolution seismic facies in a P-Cable 3D seismic survey in the Hoop area a) Uninterpreted and interpreted section in the Hoop area. The interpreted section shows the Lower Cretaceous horizons and black solid lines highlight the beddings within each seismic facies. The color code is defined in the legend and provide insights on the age of each interval. The red arrows indicate truncated reflections. b) Isopach map of Ceres, showing a U-shaped incision into the Barremian prograding unit. The position of the 3D survey is illustrated in Fig. 4, and the profile location depicted by the black solid line in Fig. 8b where major faults are shown in white framed polygons.

Fig. 9 Interpretation of high-resolution facies along three P-Cable 2D seismic profiles a) Uninterpreted (top) and interpreted (bottom) seismic profile through Apollo well (7324/2-1). The red arrows indicate truncated reflections. b) Uninterpreted (top) and interpreted (bottom) seismic profile through Atlantis well (7325/1-1). c) Uninterpreted (top) and interpreted (bottom) seismic profile, showing three incisions into the Barremian unit. The three profile locations are indicated in Fig. 4. The interpreted sections show the Lower Cretaceous horizons and black solid lines highlights the beddings within each stratigraphic unit. The legend is shown in Figs. 6, 7 and 8.

Fig. 10 Simplified evolutionary model of Ceres, a submarine channel in the Hoop area, divided into four stages. A) Stage I: Barremian. Arrival of subaqueous delta NW2. B) Stage II: Aptian. Sea level rise, sediment starvation and submarine erosion. Active channel infill with

easterly sediments. Arrival of NE-sourced lobes on the Bjarmeland Platform. C) Stage III: Early Albian. Suspension fallout and passive infill of the submarine channel. D) Stage IV: Albian. Drape with arrival of NE1. The insert drawing on the lower right of Stage II to IV illustrates the evolution of the slope gradient in the study area. The vertical dashed lines represent fictive borehole tracks of Apollo (7324/2-1) and Atlantis (7325/1-1). The figure is not-to-scale and the perspective was drawn using a vanishing point to the east. An approximate horizontal scale is given by the distance between the two wells (~ 19 km; Fig. 1)

Fig. 11 Paleo-geographic reconstruction of the study area in the SW Barents Sea at the Aptian stage. The paleo-environment around the Loppa High is modified from Marín et al. (2018) and Harishidayat et al. (2018). The black solid lines represent the main structural elements (NPD, 2017).

Fig. 2

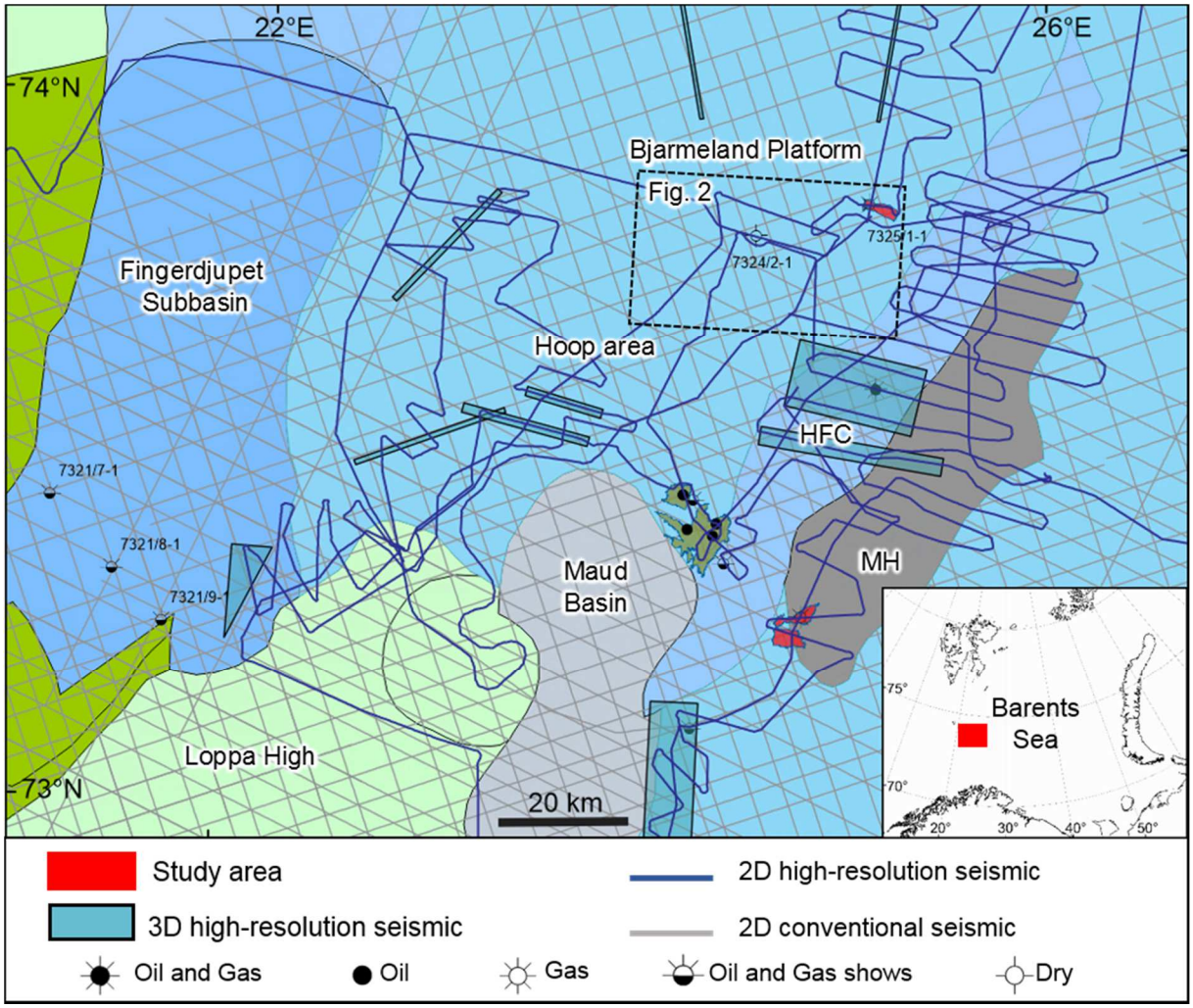
22°E
26°E
74°N
73°N
Bjarmeland Platform
Fig. 2
7325/1-1
7324/2-1
Fingerdjupet
Subbasin
Hoop area
HFC
MH
7321/7-1
7321/8-1
7321/9-1
Maud
Basin
Loppa High
20 km
Barents
Sea
75°
70°
20°
30°
40°
50°
Study area
2D high-resolution seismic
3D high-resolution seismic
2D conventional seismic
Oil and Gas
Oil
Gas
Oil and Gas shows
Dry

Fig. 1

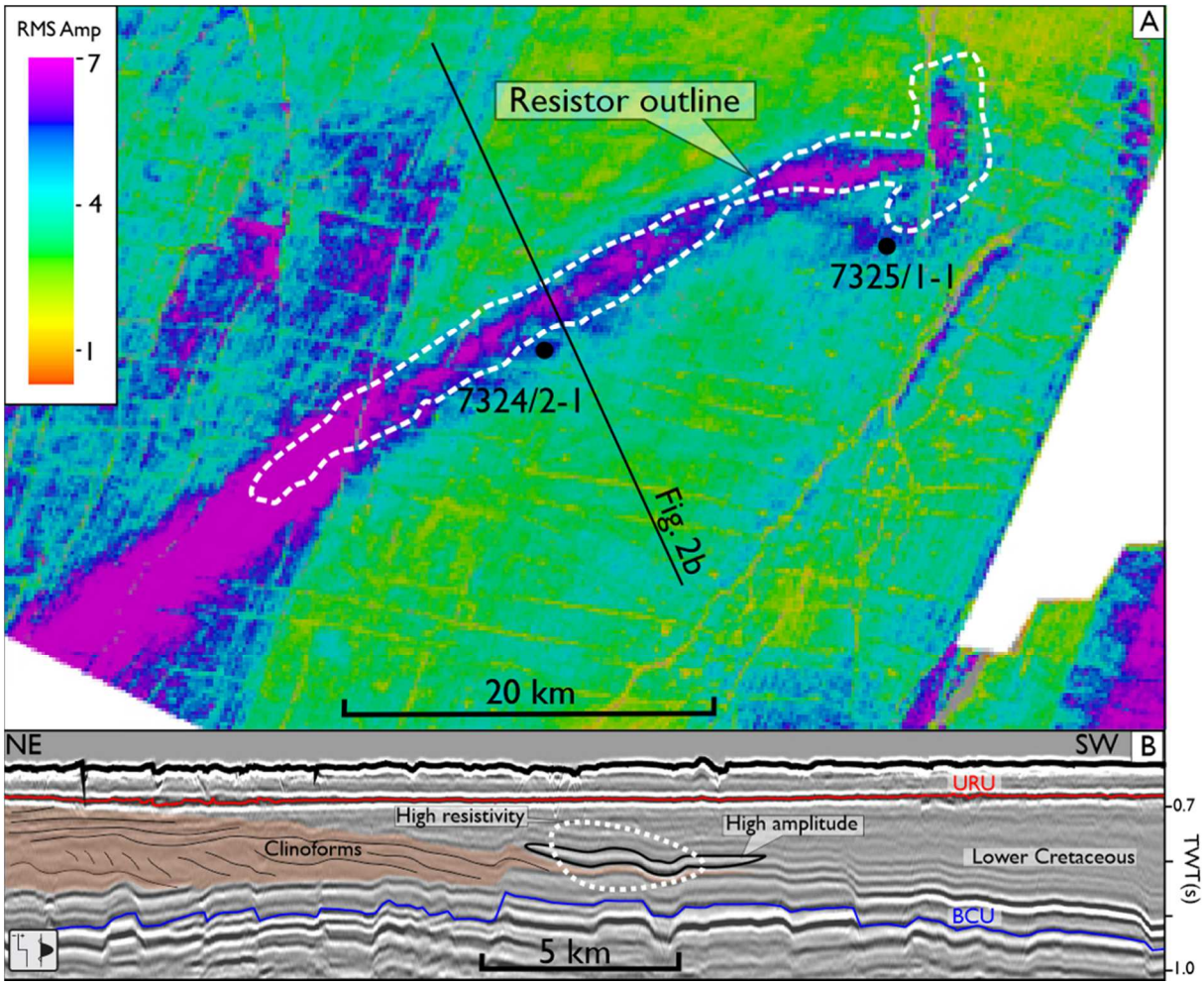
RMS Amp
7
4
1
A
Resistor outline
7325/1-1
7324/2-1
Fig. 2b
20 km
NE
SW
B
URU
High resistivity
High amplitude
Clinoforms
Lower Cretaceous
BCU
5 km
0.7
TWT(s)
1.0

Fig. 2

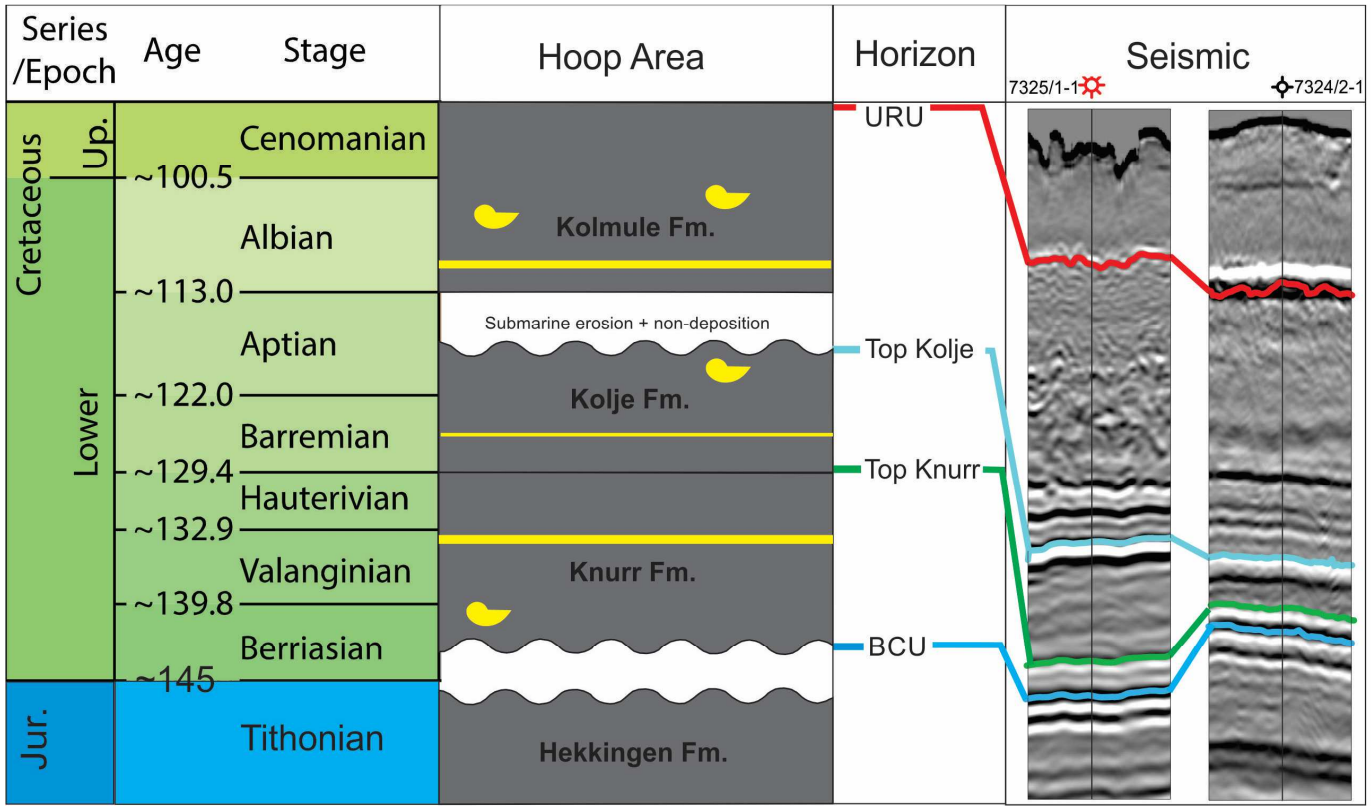
Series /Epoch
Age
Stage
Hoop Area
Horizon
Seismic
7325/1-1
7324/2-1
Cretaceous
Up.
Lower
Jur.
Cenomanian
~100.5
Albian
~113.0
Aptian
~122.0
Barremian
~129.4
Hauterivian
~132.9
Valanginian
~139.8
Berriasian
~145
Tithonian
Kolmule Fm.
Submarine erosion + non-deposition
Kolje Fm.
Knurr Fm.
Hekkingen Fm.
URU
Top Kolje
Top Knurr
BCU

Fig. 3

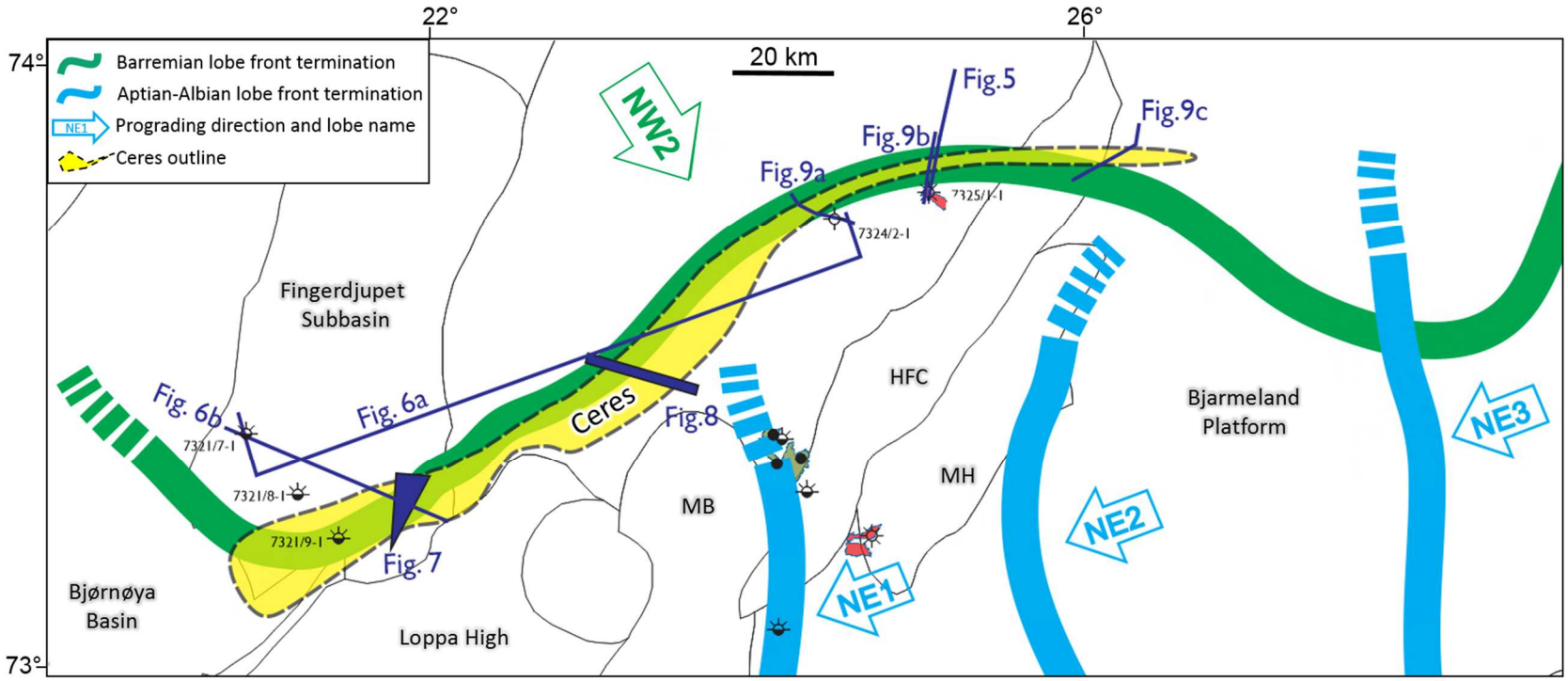
22°
26°
74°
73°
20 km
Barremian lobe front termination
Aptian-Albian lobe front termination
NE1
Prograding direction and lobe name
Ceres outline
NW2
Fig.5
Fig.9c
Fig.9b
Fig.9a
7325/1-1
7324/2-1
Fingerdjupet
Subbasin
Fig. 6b
Fig. 6a
Ceres
Fig.8
7321/7-1
7321/8-1
7321/9-1
Fig. 7
HFC
MB
MH
Bjarmeland
Platform
NE3
NE2
NE1
Bjørnøya
Basin
Loppa High

Fig. 4

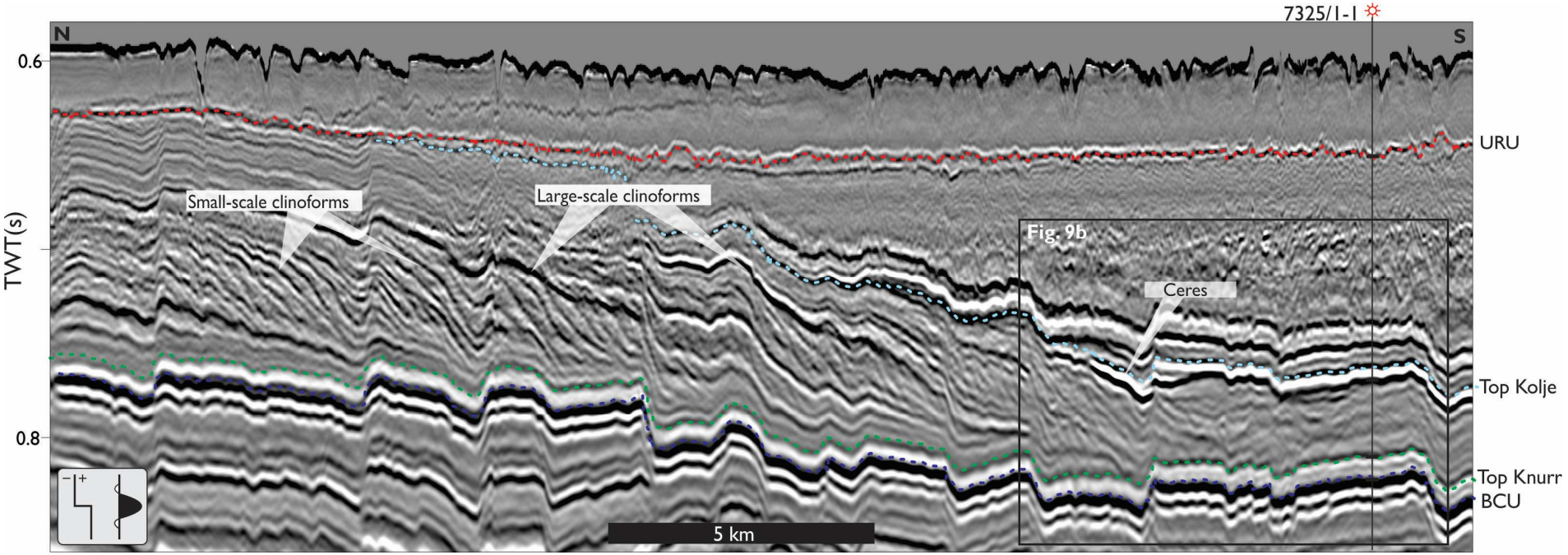
7325/1-1
N
S
0.6
0.8
TWT(s)
URU
Small-scale clinoforms
Large-scale clinoforms
Fig. 9b
Ceres
Top Kolje
Top Knurr
BCU
5 km

Fig. 5

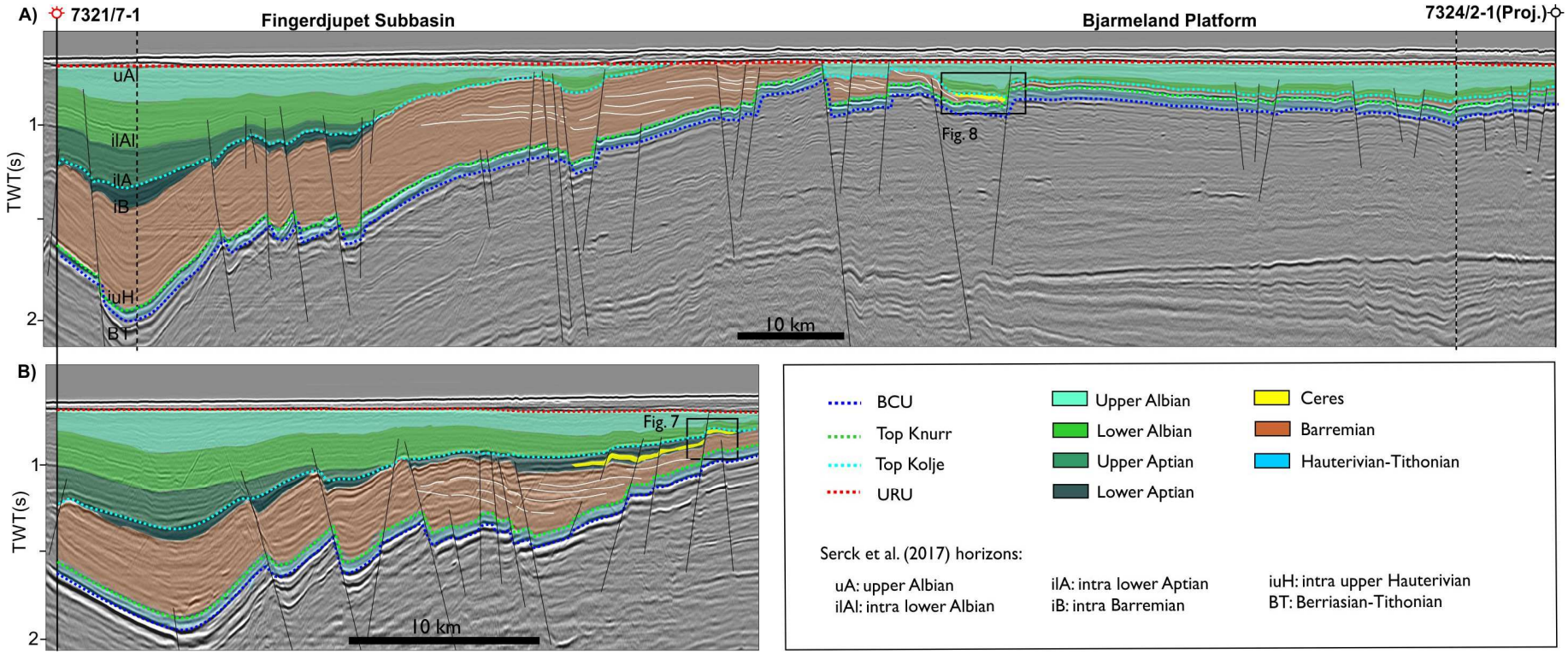
A)
7321/7-1
Fingerdjupet Subbasin
Bjarmeland Platform
7324/2-1(Proj.)
uAl
ilAl
ilA
iB
iuH
BT
TWT(s)
1
2
Fig. 8
10 km
B)
Fig. 7
10 km
BCU
Top Knurr
Top Kolje
URU
Upper Albian
Lower Albian
Upper Aptian
Lower Aptian
Ceres
Barremian
Hauterivian-Tithonian
Serck et al. (2017) horizons:
uA: upper Albian
ilAl: intra lower Albian
ilA: intra lower Aptian
iB: intra Barremian
iuH: intra upper Hauterivian
BT: Berriasian-Tithonian

Fig. 6

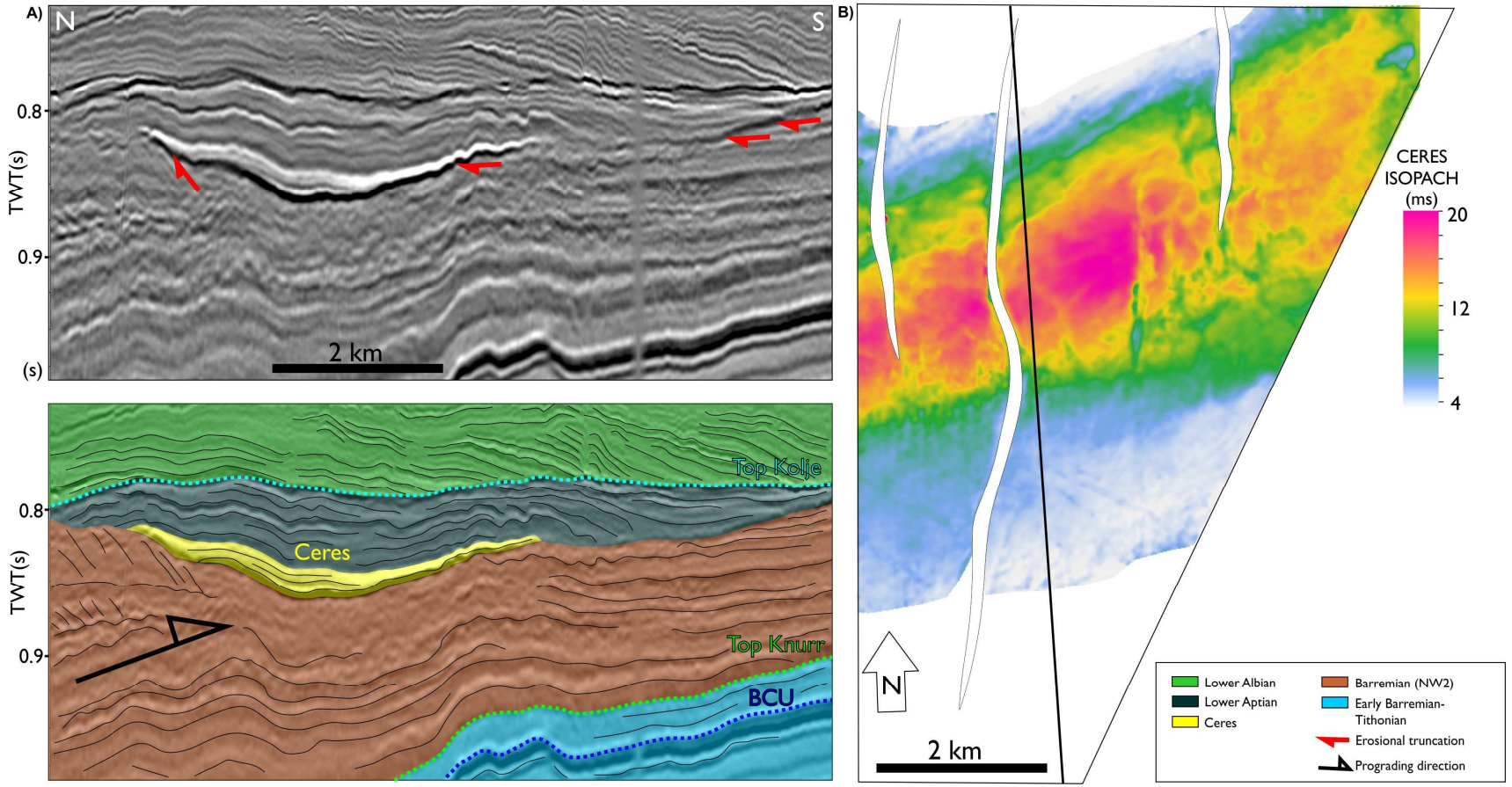
A)
N
S
0.8
TWT(s)
0.9
(s)
2 km
Top Kolje
Ceres
Top Knurr
BCU
B)
CERES
ISOPACH
(ms)
20
12
4
N
2 km
Lower Albian
Lower Aptian
Ceres
Barremian (NW2)
Early Barremian-
Tithonian
Erosional truncation
Prograding direction

Fig. 7

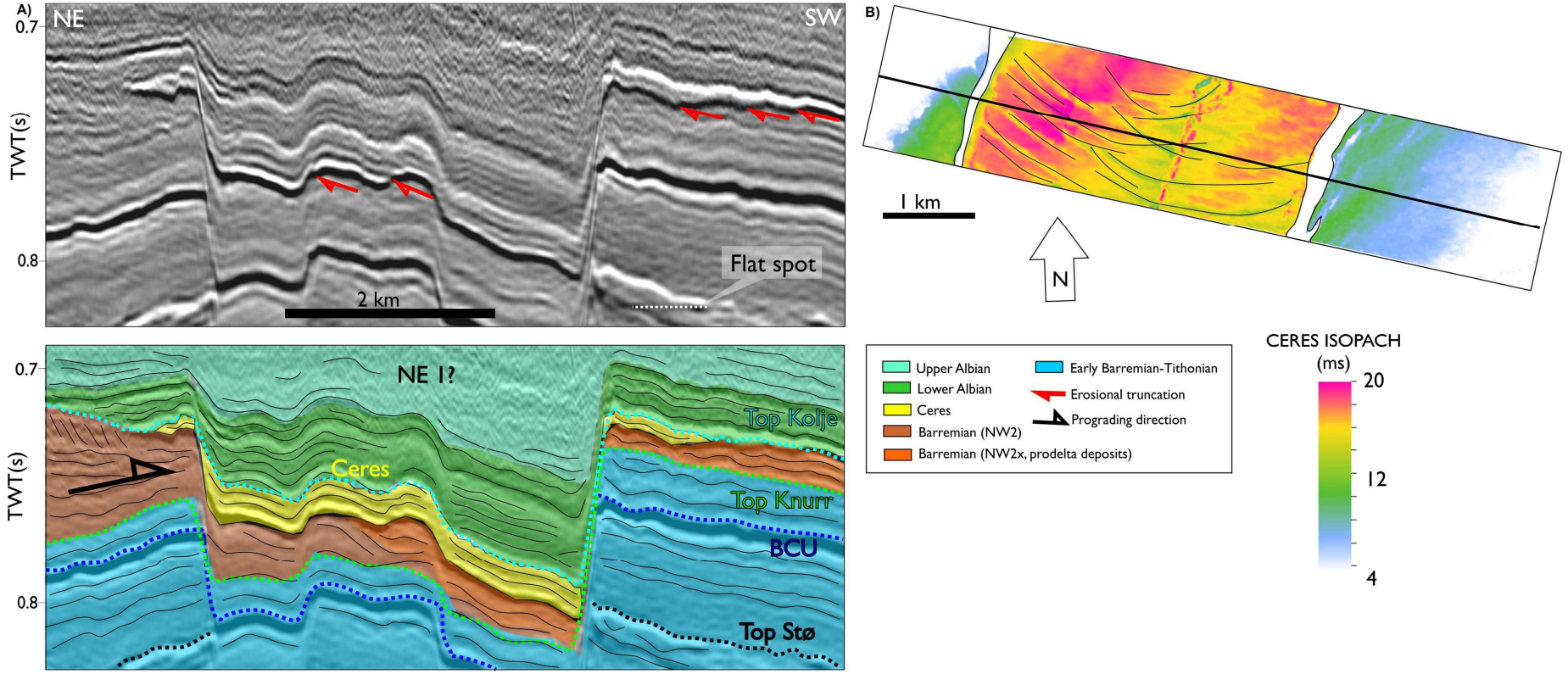
A)
NE
SW
0.7
TWT(s)
0.8
Flat spot
2 km
NE 1?
Top Kolje
Ceres
Top Knurr
BCU
Top Stø
A
B)
1 km
N
Upper Albian
Lower Albian
Ceres
Barremian (NW2)
Barremian (NW2x, prodelta deposits)
Early Barremian-Tithonian
Erosional truncation
Prograding direction
CERES ISOPACH
(ms)
20
12
4

Fig. 8

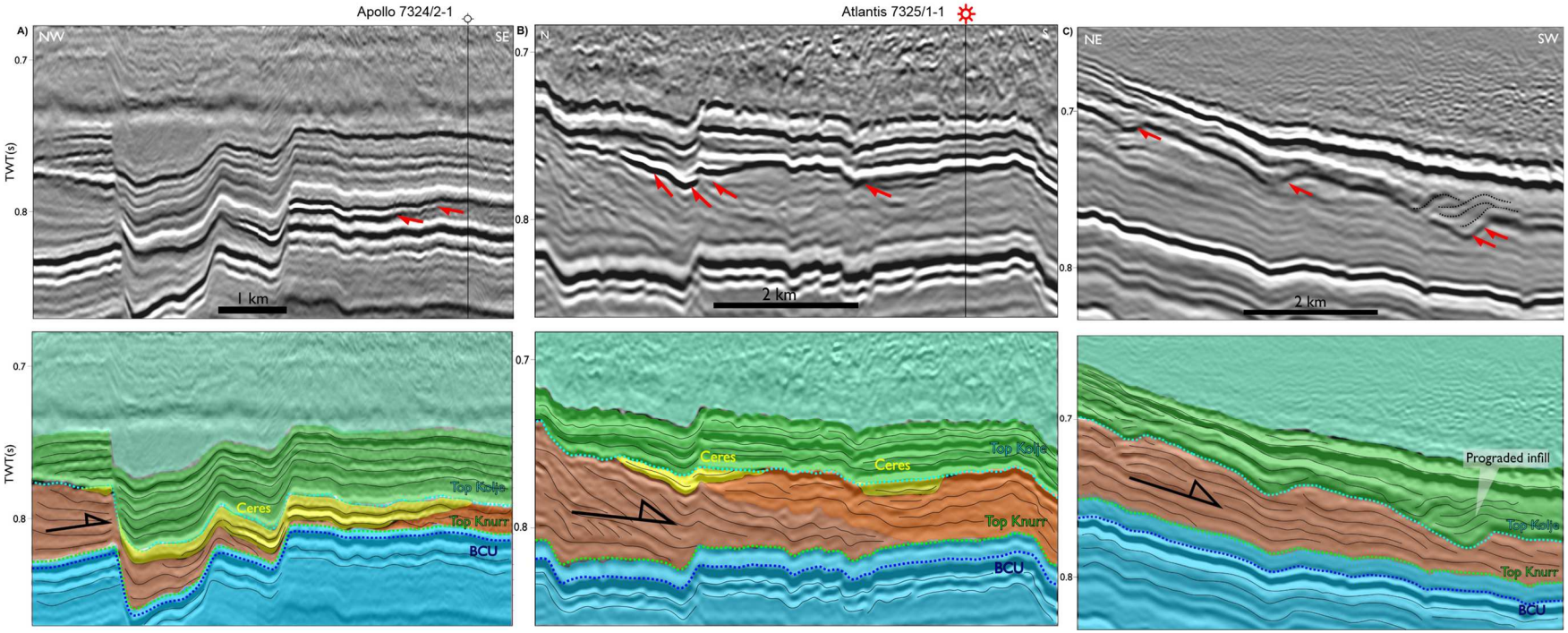
Apollo 7324/2-1
Atlantis 7325/1-1
A)
NW
SE
B)
N
S
C)
NE
SW
TWT(s)
0.7
0.8
1 km
2 km
2 km
Ceres
Top Kolje
Top Knurr
BCU
Prograded infill

Fig. 9

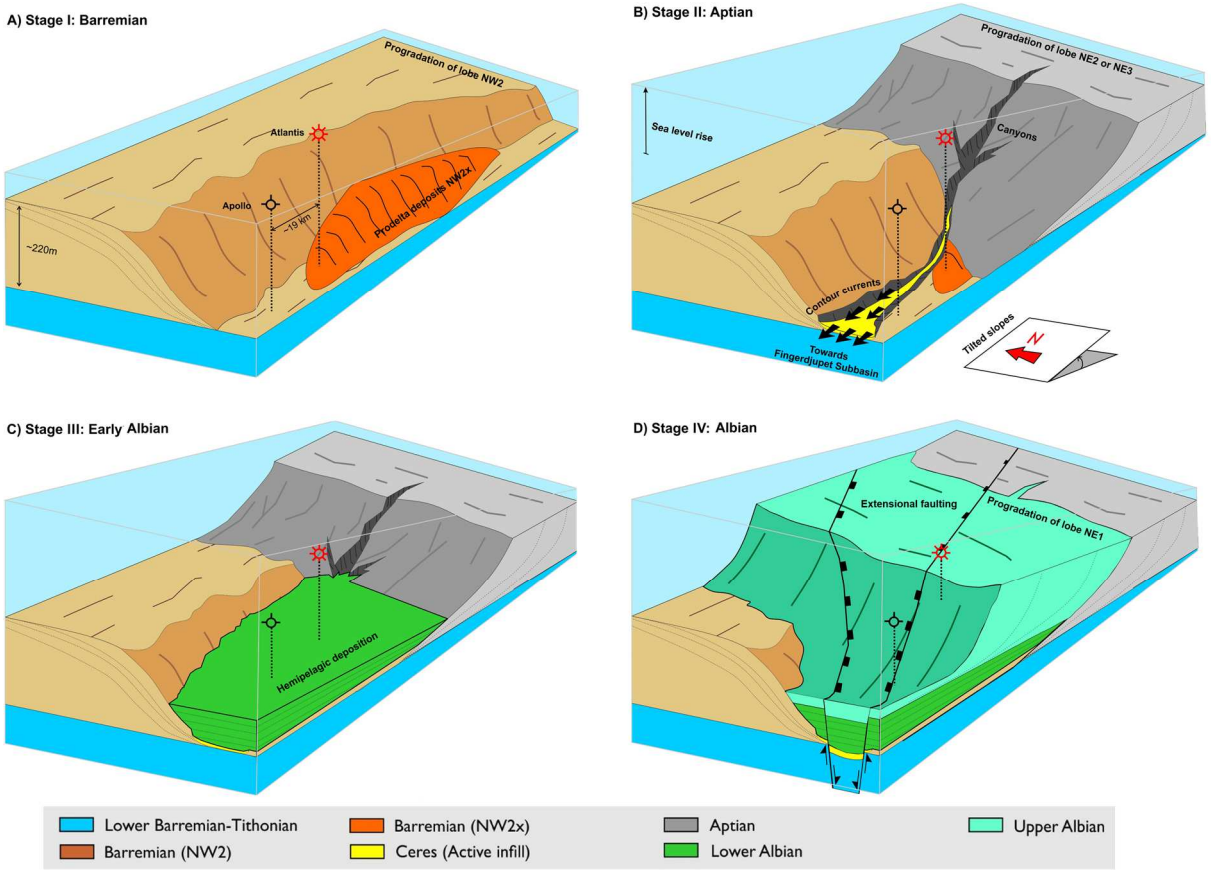
A) Stage I: Barremian
Progradation of lobe NW2
Atlantis
Apollo
~19 km
Prodelta deposits (NW2x)
~220m
B) Stage II: Aptian
Progradation of lobe NE2 or NE3
Sea level rise
Canyons
Contour currents
Towards Fingerdjupet Subbasin
Tilted slopes
N
C) Stage III: Early Albian
Hemipelagic deposition
D) Stage IV: Albian
Extensional faulting
Progradation of lobe NE1
Lower Barremian-Tithonian
Barremian (NW2)
Barremian (NW2x)
Ceres (Active infill)
Aptian
Lower Albian
Upper Albian

Fig. 10

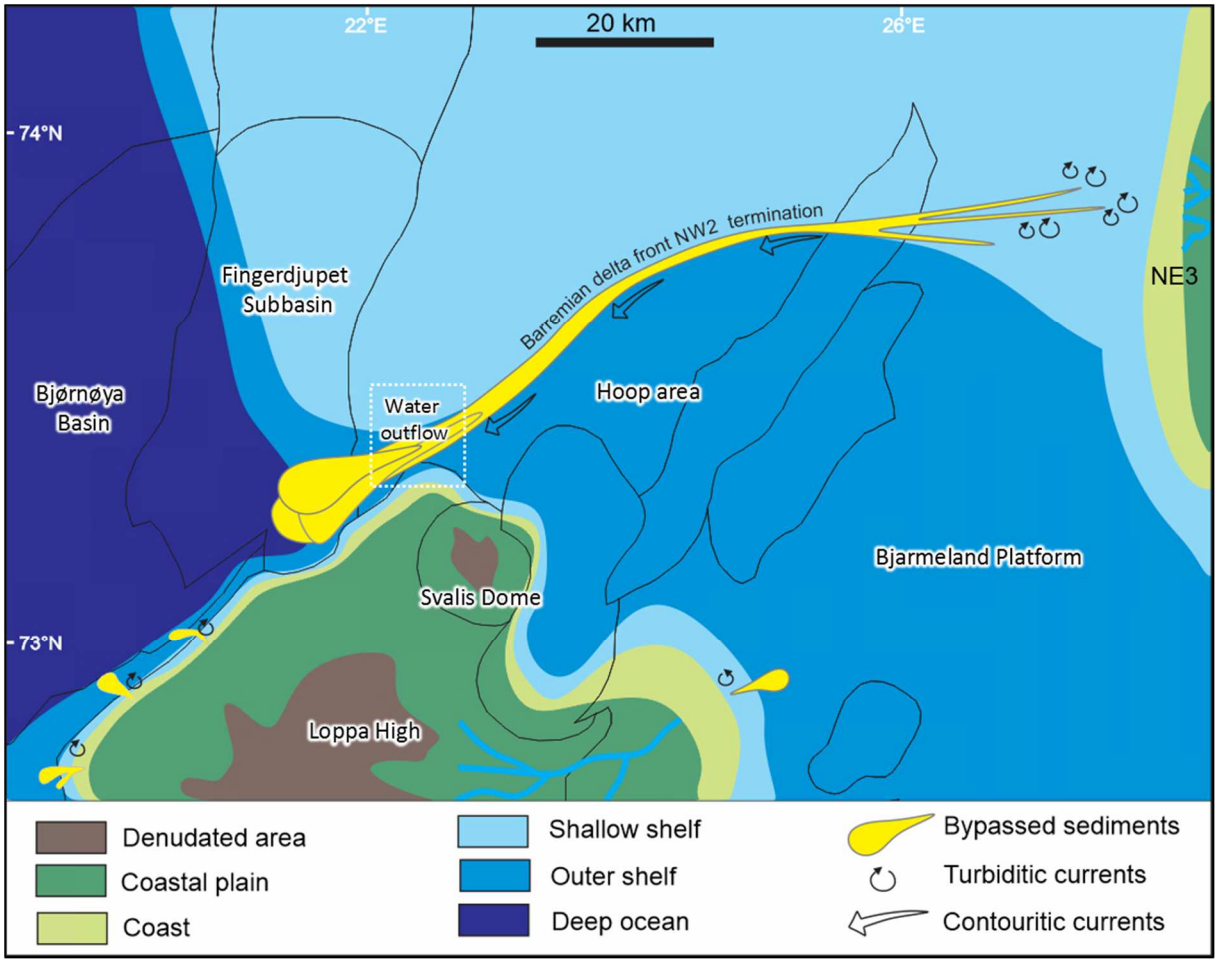
22°E
20 km
26°E
74°N
73°N
Barremian delta front NW2 termination
Fingerdjupet Subbasin
Bjørnøya Basin
Water outflow
Hoop area
NE3
Bjarmeland Platform
Svalis Dome
Loppa High
Denudated area
Coastal plain
Coast
Shallow shelf
Outer shelf
Deep ocean
Bypassed sediments
Turbiditic currents
Contouritic currents

Fig. 11